# Roles of Hyperons in Neutron Stars

Shmuel Balberg, Itamar Lichtenstadt

The Racah Institute of Physics, The Hebrew University, Jerusalem 91904, Israel

and

Gregory. B. Cook

Center for Radiophysics and Space Research, Space Sciences Building, Cornell University, Ithaca, NY 14853

#### ABSTRACT

We examine the roles the presence of hyperons in the cores of neutron stars may play in determining global properties of these stars. The study is based on estimates that hyperons appear in neutron star matter at about twice the nuclear saturation density, and emphasis is placed on effects that can be attributed to the general multispecies composition of the matter, hence being only weakly dependent on the specific modeling of strong interactions. Our analysis indicates that hyperon formation not only softens the equation of state but also severely constrains its values at high densities. Correspondingly, the valid range for the maximum neutron star mass is limited to about  $1.5-1.8~M_{\odot}$ , which is a much narrower range than available when hyperon formation is ignored. Effects concerning neutron star radii and rotational evolution are suggested, and we demonstrate that the effect of hyperons on the equation of state allows a reconciliation of observed pulsar glitches with a low neutron star maximum mass. We discuss the effects hyperons may have on neutron star cooling rates, including recent results which indicate that hyperons may also couple to a superfluid state in high density matter. We compare nuclear matter to matter with hyperons and show that once hyperons accumulate in neutron star matter they reduce the likelihood of a meson condensate, but increase the susceptibility to baryon deconfinement, which could result in a mixed baryon-quark matter phase.

Subject headings: stars: neutron — elementary particles — equation of state — stars: evolution

#### 1. Introduction

The existence of stable matter at supernuclear densities is unique to neutron stars. Unlike all other physical systems in nature, where the baryonic component appears in the form of atomic nuclei, matter in the cores of neutron stars is expected to be a homogeneous mixture of hadrons and leptons. As a result the macroscopic features of neutron stars, including some observable quantities, have the potential to illuminate the physics of supernuclear densities. In this sense, neutron stars serve as cosmological laboratories for hadronic physics. A specific feature of supernuclear densities is the possibility for new hadronic degrees of freedom to appear, in addition to neutrons and protons. One such possible degree of freedom is the formation of hyperons - strange baryons - which is the main subject of the present work. Other possible degrees of freedom include meson condensation and a deconfined quark phase.

While hyperons are unstable under terrestrial conditions and decay into nucleons through the weak interaction, the equilibrium conditions in neutron stars can make the reverse process, i.e., the conversion of nucleons into hyperons, energetically favorable. The appearance of hyperons in neutron stars was first suggested by Ambartsumyan & Saakyan (1960) and has since been examined in many works. Earlier calculations include the works of Pandharipande (1971b), Bethe & Johnson (1974) and Moszkowski (1974), which were performed by describing the nuclear force in Schrödinger theory. In recent years, studies of high density matter with hyperons have been performed mainly in the framework of field theoretical models (Glendenning 1985, Weber & Weigel 1989, Knorren, Prakash & Ellis 1995, Schaffner & Mishustin 1996, Huber at al. 1997). For a review, see Glendenning (1996) and Prakash et al. (1997). It was also recently demonstrated that good agreement with these models can be attained with an effective potential model (Balberg & Gal 1997).

These recent works share a wide consensus that hyperons should appear in neutron star (cold, beta-equilibrated, neutrino-free) matter at a density of about twice the nuclear saturation density. This consensus is attributed to the fact that all these more modern works base their estimates of hyperon-nucleon and hyperon-hyperon interactions on the experimental constraints inferred from hypernuclei. The fundamental qualitative result from hypernuclei experiments is that hyperon related interactions are similar in character and in order of magnitude to nucleon-nucleon interactions. In a broader sense, this result indicates that in high density matter, the differences between hyperons and nucleons will be less significant than for free particles.

The aim of the present work is to examine what roles the presence of hyperons in the cores of neutron stars may play in determining the global properties of these stars. We place special emphasis on effects which can be attributed to the multi-species composition of the matter while being only weakly dependent on the details of the model used to describe the underlying strong interactions.

We begin our survey in  $\S$  2 with a brief summary of the equilibrium conditions which determine the formation and abundance of hyperon species in neutron star cores. A review of the widely accepted results regarding hyperon formation in neutron stars is given in  $\S$  3. We devote  $\S$  4 to an examination of the effect of hyperon formation on the equation of state of dense matter, and the corresponding effects on the star's global properties: maximum mass, mass-radius correlations, rotation limits, and crustal sizes. In  $\S$  5 we discuss neutron star cooling rates, where hyperons might play a decisive role. A discussion of the effects of hyperons on phase transitions which may occur in high density matter is given in  $\S$  6. Conclusions and discussion are offered in  $\S$  7.

## 2. Equilibrium Conditions for Hyperon Formation Neutron Stars

In the following discussion we assume that the cores of neutron stars are composed of a mixture of baryons and leptons in full beta equilibrium (thus ignoring possible meson condensation and a deconfined quark phase - these issues will be picked up again in § 6). The procedure for solving the equilibrium composition of such matter has been describes in many works (see e.g., Glendenning (1996) and Prakash et al. (1997) and references therein), and in essence requires chemical equilibrium of all weak processes of the type

$$B_1 \to B_2 + \ell + \bar{\nu}_\ell \; ; \; B_2 + \ell \to B_1 + \nu_\ell \; ,$$
 (1)

where  $B_1$  and  $B_2$  are baryons,  $\ell$  is a lepton (electron or muon), and  $\nu$  ( $\bar{\nu}$ ) is its corresponding neutrino (anti-neutrino). Charge conservation is implied in all processes, determining the legitimate combinations of baryons which may couple together in such reactions.

Imposing all the conditions for chemical equilibrium yields the ground state composition of beta-equilibrated high density matter. The equilibrium composition of such matter at any given baryon density,  $\rho_B$ , is described by the relative fraction of each species of baryons  $x_{B_i} \equiv \rho_{B_i}/\rho_B$  and leptons  $x_\ell \equiv \rho_\ell/\rho_B$ .

Evolved neutron stars can be assumed to be transparent to neutrinos on any relevant time scale so that neutrinos are absent and  $\mu_{\nu} = \mu_{\bar{\nu}} = 0$ . All equilibrium conditions may then be summarized by a single generic equation

$$\mu_i = \mu_n - q_i \mu_e \quad , \tag{2}$$

where  $\mu_i$  and  $q_i$  are, respectively, the chemical potential and electric charge of baryon species i,  $\mu_n$  is the neutron chemical potential, and  $\mu_e$  is the electron chemical potential. Note that in the absence of neutrinos, equilibrium requires  $\mu_e = \mu_\mu$ . The neutron and electron chemical potentials are constrained by the requirements of a constant total baryon number and electric charge neutrality,

$$\sum_{i} x_{B_i} = 1 \; ; \; \sum_{i} q_i x_{B_i} + \sum_{\ell} q_{\ell} x_{\ell} = 0 \; . \tag{3}$$

The temperature range of evolved neutron stars is typically much lower than the relevant chemical potentials of baryons and leptons at supernuclear densities. Neutron star matter is thus commonly approximated as having zero temperature, so that the equilibrium composition and other thermodynamic properties depend on density alone. Solving the equilibrium compositions for a given equation of state (EOS) at various baryon densities yields the energy density and pressure which enable the calculation of global neutron star properties.

### 3. Hyperon Formation in Neutron Stars

In this section we review the principal results of recent studies regarding hyperon formation in neutron stars. The masses, along with the strangeness and isospin, of nucleons and hyperons are given in Tab. 1. The electric charge and isospin combine in determining the exact conditions for each hyperon species to appear in the matter. Since nuclear matter has an excess of positive charge and negative isospin, negative charge and positive isospin are favorable along with a lower mass for hyperon formation, and it is generally a combination of the three that determines the baryon density at which each hyperon species appears. A quantitative examination requires, of course,

modeling of high density interactions. We begin with a brief discussion of the current experimental and theoretical basis used in recent studies that have examined hyperon formation in neutron stars.

## **3.1.** Experimental and Theoretical Background

The properties of high density matter chiefly depend on the nature of the strong interactions. Quantitative analysis of the composition and physical state of neutron star matter are currently complicated by the large uncertainties regarding strong interactions, both in terms of the difficulties in their theoretical description and from the limited relevant experimental data. None the less, progress in both experiment and theory have provided the basis for several recent studies of the composition of high density matter, and in particular suggests it will include various hyperon species.

Experimental data from nuclei set some constraints on various physical quantities of nuclear matter at the nuclear saturation density,  $\rho_0 = 0.16$  fm<sup>-3</sup>. Important quantities are the bulk binding energy, the symmetry energy of non-symmetric matter (i.e., different numbers of neutrons and protons), the nucleon effective mass in a nuclear medium, and a reasonable constraint on the compression modulus of symmetric nuclear matter. However, at present, little can be deduced regarding properties of matter at higher densities. Heavy ion collisions have been able to provide some information regarding higher density nuclear matter, but the extrapolation of these experiments to neutron star matter is questionable since they deal with hot non-equilibrated matter.

Relevant data for hyperon-nucleon and hyperon-hyperon interactions is more scarce, and relies mainly on hypernuclei experiments (for a review of hypernuclei experiments, see Chrien & Dover (1989), Gibson & Hungerford (1995)). In these experiments a single hyperon is formed in a nucleus, and its binding energy is deduced from the energetics of the reaction (typically meson scattering such as  $X(K^-, \pi^-)X$ ).

There exists a large body of data for single  $\Lambda$ -hypernuclei, which clearly shows bound states of a  $\Lambda$  hyperon in a nuclear medium. Millener, Dover & Gal (1988) used the nuclear mass dependence of  $\Lambda$  levels in hypernuclei to derive the density dependence of the binding energy of a  $\Lambda$  hyperon in nuclear matter. In particular, they estimate the potential depth of a  $\Lambda$  hyperon in nuclear matter at density  $\rho_0$  to be about -28 MeV, which is about one third of the equivalent value for a nucleon in symmetric nuclear matter. The data from  $\Sigma$ -hypernuclei are more problematic (see below). A few emulsion events that have been attributed to  $\Xi$ -hypernuclei seem to suggest an attractive  $\Xi$  potential in a nuclear medium, somewhat weaker than the  $\Lambda$ -nuclear matter potential.

A few measured events have been attributed to the formation of double  $\Lambda$  hypernuclei, where two  $\Lambda$ 's have been captured in a single nucleus. The decay of these hypernuclei suggests an attractive  $\Lambda$ – $\Lambda$  interaction potential of 4–5 MeV (Bodmer & Usmani 1987), somewhat less than the corresponding nucleon-nucleon value of 6–7 MeV. This value of the  $\Lambda$ – $\Lambda$  interaction is often used as the baseline for assuming a common hyperon-hyperon potential, corresponding to a well depth for a single hyperon in isospin-symmetric hyperon matter of -40 MeV. While this value should be taken with a large uncertainty, the typical results regarding hyperon formation in neutron stars are generally insensitive to the exact choice for the hyperon-hyperon interaction, as discussed below.

We emphasize again that the experimental data is far from comprehensive, and great uncertainties still remain in the modeling of baryonic interactions. This is especially true regarding densities

greater than  $\rho_0$ , where the importance of many body forces increases. Three body interactions are used in some nuclear matter models (Wiringa, Fiks & Fabrocini 1988, Akmal, Pandharipande & Ravenhall 1998). Many-body forces for hyperons are currently difficult to constrain from experiment (Bodmer & Usmani 1988), although some attempts have been made on the basis of light hypernuclei (Gibson & Hungerford 1995). Indeed, field theoretical models include a repulsive component in the two-body interactions through the exchange of vector mesons, rather than introduce explicit many body terms. We note that the effective equation used here is also compatible with theoretical estimates of  $\Lambda$ NN forces through the repulsive terms it includes (Millener, et al. 1988).

In spite of these significant uncertainties, the qualitative conclusion that can be drawn from hypernuclei is that hyperon-related interactions are similar both in character and in order of magnitude to the nucleon-nucleon interactions. Thus nuclear matter models can be reasonably generalized to include hyperons as well. In recent years this has been performed mainly with relativistic theoretical field models, where the meson fields are explicitly included in an effective Lagrangian. A commonly used approximation is the relativistic mean field (RMF) model following Serot & Walecka (1980), and implemented first for multi-species matter by Glendenning (1985), and more recently by Knorren et al. (1995) and Schaffner & Mishustin (1996) (see the recent review by Glendenning (1996)). A related approach is the relativistic Hartree-Fock (RHF) method that is solved with relativistic Green's functions (Weber & Weigel 1989, Huber at al. 1997). Balberg & Gal (1997) demonstrated that the quantitative results of field theoretical calculations can be reproduced by an effective potential model.

The results of these works provide a wide consensus regarding the principal features of hyperon formation in neutron star matter. This consensus is a direct consequence of incorporating experimental data on hypernuclei (Balberg & Gal 1997). These principal features are discussed below.

## **3.2.** Estimates for Hyperon Formation in Neutron Stars

Hyperons can form in neutron star cores when the nucleon chemical potentials grow large enough to compensate for the mass differences between nucleons and hyperons, while the threshold for the appearance of the hyperons is tuned by their interactions. The general trend in recent studies of neutron star matter is that hyperons begin to appear at a density of about  $\rho_B = 2\rho_0$ , and that by  $\rho_B \approx 3\rho_0$  hyperons sustain a significant fraction of the total baryon population. An example of the estimates for hyperon formation in neutron star matter, as found in many works, is displayed in Fig. 1. The equilibrium compositions - relative particle fractions  $x_i$  - are plotted as a function of the baryon density,  $\rho_B$ . These compositions were calculated with case 2 of the effective equation of state detailed in the appendix, which is similar to model  $\delta = \gamma = \frac{5}{3}$  of Balberg & Gal (1997). Figure 1a presents the equilibrium compositions for the "classic" case of nuclear matter, when hyperons are ignored, and matter is composed of nucleons and leptons. The equilibrium compositions when hyperons are included are shown in Fig. 1b, when the interaction of  $\Sigma$  hyperons in nuclear matter (nm) is set to be equal to the  $\Lambda$ -nm case (except for the inclusion of isospin dependent components in the  $\Sigma$ -nm case). Key qualitative aspects of hyperon formation in neutron star matter are:

1. The first hyperon species that appears is the  $\Sigma^-$ , closely followed by the  $\Lambda$ . The negative

charge of the  $\Sigma^-$  outweighs the 80 MeV mass difference, as a result of the more lenient condition of Eq. (2) that requires  $\mu_{\Lambda} = \mu_n$  but  $\mu_{\Sigma^-} = \mu_n + \mu_e$ . However, the formation of  $\Sigma^-$  hyperons is quickly moderated by the isospin dependent forces that disfavor an excess of  $\Sigma^-$ 's over  $\Sigma^+$ 's, and also joint excess of  $\Sigma^-$ 's and neutrons (both of negative isospin projection). Thus, the  $\Sigma^-$  fraction saturates at about 0.1, while the  $\Lambda$ 's, free of isospin-dependent forces, continue to accumulate until short range repulsion forces cause them to saturate as well.

- 2. Other hyperon species follow at higher densities. Under the assumptions of the particular model of EOS 2, other Σ's generally appear before the Ξ's due to the large mass difference, but the Ξ<sup>-</sup> becomes favored due to its negative electric charge and quickly becomes abundant in the matter.
- 3. A unique aspect of hyperon accumulation is the immediate deleptonization of the matter. Leptons are rather expensive in terms of energy density (and pressure), and survive in nuclear matter only in order to maintain charge neutrality with the protons. Hyperons offer an option for lowering the neutron excess free of lepton formation, and the negatively charged hyperons allow charge neutrality to be maintained within the baryon community. The lepton fraction is therefore reduced by hyperon formation, and the appearance of the Ξ<sup>-</sup> is followed by a very powerful deleptonization. The muon population is completely extinguished, and the electron fraction drops below 1%, whereas it exceeds 10% in the nuclear matter case.

We remark that some of these general features are somewhat dependent on the assumptions used to describe the hyperon-nucleon interactions. In particular, if any reaction is changed to be highly repulsive, the formation of some species may become suppressed. As an example, Fig. 1c shows the equilibrium compositions found when a strongly repulsive component is introduced in the potential of  $\Sigma$  hyperons in nuclear matter. The existence of such a repulsive isoscalar component has been suggested on the basis of recent analysis of  $\Sigma^-$  atoms (Batty, Friedman & Gal 1994, Mareš et al. 1995). The analysis predicts a  $(\Sigma-nm)$  repulsion of several MeV at the nuclear saturation density, and even larger repulsion at greater densities. If such repulsion exists,  $\Sigma$ 's do not form in neutron star matter (see also Knorren et al. 1995, Balberg & Gal 1997). As a result, A formation begins at slightly lower densities than when  $\Sigma$ 's are present, and  $\Xi$  formation is especially enhanced. It is noteworthy, however, that the overall strangeness fraction in this case is similar to the case when  $\Sigma$ 's are present. Since at least the  $\Lambda$ -nm interaction seems well determined, we believe a significant change of the basic features of hyperon formation is unlikely (see also the analysis by Glendenning & Moszkowski (1991)). There is less dependence on the hyperon-hyperon interactions (again, unless they are set to be highly repulsive - which seems unlikely in view of data from double  $\Lambda$  hypernuclei). This is because the matter is dominated by nucleons until high densities, where universal short range forces are expected to take precedence over the specific baryon identities.

We note in passing that  $\Delta$  isobars are also candidates for formation in high density matter. Most works which examined the possible appearance of  $\Delta$  isobars in dense matter find that they are never present, due to a strong isovector repulsion. It should be noted that in some relativistic Hartree-Fock frameworks the nucleon- $\Delta$  coupling (through the  $\rho$ -meson) is significantly weakened, and  $\Delta$  isobars are found to appear in high density neutron star matter (Weber & Weigel 1989, Huber at al. 1997). In this work we follow the assumption that  $\Delta$ 's do not appear in neutron star matter.

To conclude, it is noteworthy that recent works agree that hyperons appear at a density of about  $2\rho_0$ , and at higher densities the matter will possess a sizable hyperon fraction, coupled to significant deleptonization. We emphasize again that these qualitative features are common to all works which examined hyperon formation in neutron star matter and are only weakly dependent on the specifics of the underlying models. These models are based on various types of approximations and are limited by the large uncertainties involved; clearly, further work (and, hopefully, more experimental data) is required to obtain more reliable quantitative results. None the less, this consensus is a direct consequence of employing data from hypernuclei experiments, and therefore may serve as valid indication regarding hyperon abundances in high density matter at beta-equilibrium. In the following analysis we assume that these recent works do provide a basis for the investigation of the effects of hyperon formation on global properties of neutron stars.

### 4. Roles of Hyperons in the Equation of State

The most significant implications of the composition of high density matter for the global properties of neutron stars are reflected in the equation of state (EOS). It is the EOS which determines the mass and radius a neutron star can hold for a given central density, and what effect rotation will have on these values. In turn, the observed constraints on the maximum mass and rotational frequencies of pulsars can provide indirect clues regarding the physics of high density matter.

The principal effect caused by hyperon formation in the dense core of neutron stars is a softening of the EOS. The softening is seen when compared against the EOS for matter composed of nucleons and leptons alone, but with otherwise identical assumptions regarding the strong interactions. This basic property of matter with hyperons has been noted in many works (Glendenning 1996, and references therein), and is a fundamental result that is basically independent of the precise model used for the baryonic interactions. Hyperons offer another degree of freedom for baryonic matter, and relieve some of the Fermi pressure of the nucleons. The creation of additional species allows energy to be held as mass rather than kinetic and potential energy, which are more expensive in terms of pressure. Here we wish to call attention to some of the underlying features of hyperon induced softening.

It is useful to begin with an emphasis on the fundamental relation between the microscopic baryonic interactions and the macroscopic EOS. As demonstrated explicitly by Pandharipande, Pines & Smith (1976), the nuclear matter EOS is critically coupled to the nucleon-nucleon interaction: the greater the short range repulsion, the greater the energy density for a given baryon density, and hence a stiffer EOS. Since there are practically no experimental limits on the short range repulsion, published nuclear matter equations vary over a relatively large range.

The microscopic-macroscopic connection becomes even more pronounced when hyperons are taken into account. As discussed in detail by Balberg & Gal (1997), the nucleon-nucleon interaction also determines the rate at which the nucleon chemical potential rises with increasing density. Since the nucleon chemical potentials determine the amount of hyperon accumulation in the matter according to the conditions of Eq. (2), strong short range nucleon-nucleon repulsion enhances hyperon formation, which has a softening effect on the EOS. Hence, hyperon formation induces a fundamental balance between the microscopic equilibrium compositions and the macroscopic

properties of the EOS, which restrains the resulting equation to a relatively narrow range of values. Hyperon formation therefore serves as a "pressure control" mechanism in high density matter.

We demonstrate the "pressure control" induced by hyperons by comparing two equations of state which are significantly different in their description of baryon-baryon interactions. Both are based on the effective EOS of Balberg & Gal (1997) (see appendix). EOS 1 is moderately stiff, and has an incompressibility of K=240 MeV for symmetric nuclear matter at density  $\rho_0$ , which is the commonly used value. EOS 2 is stiff, with K=320 MeV. The calculated equations of state for matter in beta-equilibrium are plotted in Fig. 2; plotted are the EOS for (i) matter with nucleons and leptons alone, (ii) matter with nucleons, hyperons and leptons, and (iii) matter with nucleons, hyperons and leptons, but when  $\Sigma$  hyperons are absent from the matter (i.e., a strongly repulsive  $\Sigma$ -nm interaction is assumed).

The pressure control discussed above can be understood from the qualitative difference between the respective equations of model 1 and model 2. In the nuclear matter case (top solid line and dashed line), EOS 2 is stiffer than EOS 1 through the entire density range since it is based on a more powerful short range repulsion between nucleons. No further degrees of freedom exist, and the difference between the two equations grows unhindered. A qualitatively different picture arises when comparing the two equations if all hyperon species are allowed to appear (thick solid curve and thick dashed curve for EOS 1 and 2 respectively). The stronger repulsion between nucleons in EOS 2 enhances hyperon accumulation, resulting in a more pronounced softening effect. Hyperon formation actually causes EOS 2 to become softer over some density interval, and in general confines both equations to a narrower range of values.

It is also noteworthy that a similar pressure control is achieved when  $\Sigma$  hyperons are extinct (dot-dashed lines). Suppressing  $\Sigma$  formation eliminates some degrees of freedom and the resulting EOS is naturally stiffer than when all hyperon species appear, implying that the EOS depends on the number of available species (Knorren et al. 1995, Balberg & Gal 1997). None the less, the remaining hyperons maintain enough degrees of freedom to allow for the manifestation of the basic feature of pressure control.

Similar trends of pressure control are found for other variations of the effective EOS (Balberg & Gal 1997), and may also be inferred from other works which compared equations of state (Glendenning 1985, Schaab et al. 1997). This is yet another consequence of the common basis used for the hyperon-nucleon interactions, and the same reservations made about hyperon formation apply here as well: if the hyperon-nucleon interactions at higher densities are radically different than those inferred from hypernuclei, the pressure regulation effect could be lost.

In conclusion, we emphasize that "pressure control" is a fundamental result of the availability of new baryonic degrees of freedom. Since the bulk of the matter in neutron stars is at a density close to that of the core, the softening of the EOS and the hyperon induced pressure control have immediate consequences on the global properties of these stars. These consequences are discussed in the following subsections.

## **4.1.** The Maximum Mass

The most fundamental role played by the high density EOS is in determining the relation between the star's central density and its mass and radius. Calculating the mass as a function of the central density yields a mass sequence for a given EOS and these sequences provide a convenient measure for comparing different equations. Of special importance is the maximum mass each equation predicts, since it serves as an integral measurement of the properties of the equation.

We begin with an examination of static (non-rotating) sequences for the different equations of state, by integrating the Tolman-Oppenheimer-Volkoff equations, namely

$$\frac{dm}{dr} = 4\pi r^2 \varepsilon \; ; \quad \frac{dP}{dr} = -\frac{Gm\varepsilon}{r^2} \left( 1 + \frac{P}{c^2 \varepsilon} \right) \left( 1 + \frac{4\pi r^3 P}{c^2 m} \right) \left( 1 - \frac{2Gm}{c^2 r} \right)^{-1} \; , \tag{4}$$

where  $\varepsilon$  is the energy density (in gm/cm<sup>3</sup>) and P is the pressure (in dyne/cm<sup>2</sup>). The integration is performed following the recipe of Arnett and Bowers (1977). For subnuclear densities we use the EOS of Feynman, Metropolis & Teller (1949), followed by that of Baym, Pethick & Sutherland (1971) up to the neutron drip density, and the equation of Baym, Bethe & Pethick (1971) up to nuclear matter density. We typically interpolate over a small region when connecting different equations (while the choice of interpolation limits is somewhat arbitrary, the resulting neutron star properties usually show very low sensitivity to these limits).

The resulting mass sequences are shown in Fig. 3. The onset of hyperon formation can be identified clearly for every EOS as the irregularities in each curve. The softening induced by the formation of hyperons is also easily identified, since it enforces - for any given central density - a lower neutron star mass than the mass found for nuclear matter with an equivalent EOS.

Correspondingly, the maximum mass found with an EOS which includes hyperons is naturally lower than when hyperons are neglected. Again, this is a general result of allowing more baryon species to appear in the matter, regardless of the specifics of the model used for the strong interactions (and, indeed, it is noted in all works which included hyperon formation in neutron star matter). A more subtle effect concerning neutron star masses is the theoretical limit that the inclusion of hyperons forces on the range of values of the maximum mass. This can also be seen in Fig. 3, where the different equations with hyperons yield maximum masses which lie in a rather narrow range:  $1.5-1.8~M_{\odot}$ .

Limiting the range for the maximum mass is not unique to the specific equations used in this work. As was first demonstrated in the framework of RMF models (Glendenning & Moszkowski 1991), this restriction basically arises from constraining the hyperon-related interactions by hypernuclei experimental data. We emphasize here that the underlying principal reason for this maximum mass constraint is the hyperon-induced pressure control discussed above, and therefore is, in essence, model independent. This conclusion is further supported by a survey of maximum masses found in various works where hyperons were included in high density matter: a large majority of these works (see the reviews by Glendenning 1996 and Prakash et al. 1997) place the maximum static mass in a narrow range of  $1.5-2.0~M_{\odot}$ , with the upper limit being reached only with equations that are extremely stiff at  $\rho \approx \rho_0$ . Since no "pressure control" is available for nuclear matter equations of state, the theoretical limit they provide on the static maximum mass is much weaker: roughly  $1.5-2.7~M_{\odot}$  (Cook, Shapiro & Teukolsky 1994).

Unfortunately, the current observational constraint is only that  $M_{max} \geq 1.44 \ M_{\odot}$  (the well determined mass of pulsar 1913+16). This constraint allows almost all theoretical equations of state to be considered legitimate. The fact that larger mass pulsars have not been observed may indicate that the maximum mass is indeed low, and several arguments have been made in support of this possibility (Bethe & Brown 1995). On the other hand, should a large mass neutron star be

observed, it will prove extremely valuable in ruling out different equations of state. Currently, the Vela pulsar is the only likely candidate for a large mass pulsar (Van Kerkwijk, M. 1997, private communication), but the uncertainties in determining its mass are still very large. It should be noted that recently measured kilohertz Quasi-Periodic-Oscillations (QPO's) in X-ray binaries (van der Klis 1997) may also provide tighter constraints on the value of the maximum mass, since the underlying neutron star is known to be accreting.

### **4.2.** *Radii*

Solutions of the Tolman-Oppenheimer-Volkoff equations relate the radius of a neutron star to its mass for any given EOS. Broadly speaking, the radius of the neutron star is a poor indicator of the properties of the inner core ( $\rho_B \ge 2\rho_0$ ). While this inner core holds most of the mass of a  $\sim 1.4~M_{\odot}$  star for almost any EOS, it only extends to about half of the star's radius. The radius is far more dependent on the EOS at  $\rho_B \sim \rho_0$  and below, which is indifferent to the possible appearance of new degrees of freedom in the core. Never the less, some qualitative observations regarding possible effects of hyperon formation on neutron star radii can still be made.

Figure 4 compares the mass-radius dependence of static neutron stars for various published equations of state which do not include hyperons to those of EOS 1 and 2 with all types of hyperons. The nuclear matter equations are FPS (Lorenz, Ravenhall & Pethick 1993), L (Mean-field EOS by Pandharipande & Smith 1975), A (Reid soft-core by Pandharipande 1971b), and AU (Wiringa, Fiks & Fabrocini 1988), where we follow the notation of Cook et al. (1994). The radii at low masses  $(M \le 1 M_{\odot})$  are basically dependent only on the EOS below  $2\rho_0$ , and the differences between the radii for various equations of state in this region reflect the differences regarding nuclear matter at these densities. For masses close to the maximum mass for each equation, the radius is naturally smaller and the star is typically more compact when the high density EOS is softer.

One effect that does stand out concerning the equations with hyperons is that there is a larger difference between the typical radii for a low mass star and the radius of the maximum mass configuration than in other equations. Comparing the radius of a 1.4  $M_{\odot}$  star and the radius for the maximum mass star yields a difference of 3.5 km and 3.4 km for EOS 1 and 2, respectively. For the other equations this difference does not exceed 2.5 km. This is a result of the specific contrast in the equations with hyperons used here, which are moderately stiff to stiff at lower densities, and soft (due the effect of hyperons) at higher densities. Clearly, such an effect will be common to any EOS which follows such a change from low to high densities; however, hyperon formation offers a natural explanation for such a trend, if it indeed exists. It should also be noted that a large difference between the radii at 1.4  $M_{\odot}$  and at maximum mass is not a necessary consequence of hyperon formation, and would not have been found if the EOS was softer at low densities.

Unfortunately, current observations of neutron stars do not provide radius measurements to any useful precision. There is no reason to infer either presence or absence of a large difference between the radius for  $M=1.4\,M_{\odot}$  and  $M\lesssim M_{max}$ , which is not known in any case (however, as discussed below, interpretation of pulsar glitches may serve as an indication that the equation of state does change from stiff at low densities to softer at higher ones). We note that future analysis of QPO's might hold significant potential for establishing mass radius relationships for accreting objects, although accurate measurement of the neutron star rotation and its effect on the stellar

shape are required (Miller, Lamb & Cook 1998).

#### **4.3.** Rotation Periods and Limits

Constraints on the high density EOS can be derived from the maximal observed angular velocity of pulsars, from the properties of their rotational evolution (spin down), and from mass-angular velocity relations that have been established for a few pulsars. Very rapid rotation ( $\Omega \ge 3 \times 10^4 \text{ s}^{-1}$ ), if observed, will serve as an important component in determining the structure of a neutron star (Lattimer et al. 1990). Note that rotational limits and deformation must be treated self-consistently in the framework of general relativity.

In Fig. 5 we show the dependence of the angular velocity,  $\Omega$ , of a neutron star on its angular momentum, J, calculated with the formalism presented by Cook et al. (1994) with EOS 2. The figure describes the star's rotational evolution as it slows down by radiating energy and angular momentum. The evolutionary sequence of a "normal" star of constant rest mass (solid lines) proceeds from the mass shed limit (dashed line on the right) to the static limit (the origin) by losing angular momentum. As with all equations of state (Cook et al. 1994), there are also "supramassive" sequences, where the rest mass is too large to allow a stable static solution. A supramassive sequence is meta-stabilized by sufficiently rapid rotation, and will collapse to a black hole at some point in its evolution. The onset of collapse (instability to quasi-radial perturbations) corresponds to the stability limit, denoted by the thin dashed line in the figure.

We call attention to the fact that for EOS 2 there are "normal" sequences that show spin-up of the neutron star during some part of the sequence. Spin up must occur in the super-massive sequence, since their unstable portions are always at higher angular velocity than the stable portion for the same value of angular momentum (Cook et al. 1994). On the other hand, spin up of a normal sequence is unusual in equations of state for nuclear matter, but is possible once hyperons are included.

Loss of angular momentum causes the star to both lose rotational energy, and contract and become more spherical. The balance of these two effects usually results in a decrease of the angular velocity, but an increase is also possible if the EOS is sufficiently soft over a large region of the star. In Newtonian physics the condition is that the effective adiabatic index of the star is less than  $\frac{4}{3}$ , and when general relativity is included, even slightly above this value (Cook, Shapiro & Teukolsky 1992). In Fig. 6 we show the adiabatic index,  $\gamma = d\log(P)/d\log(\rho)$  for EOS 2 and the EOS with hyperons of Glendenning (1996, pg. 244). The effect of hyperons on the equations is obvious, as  $\gamma$  drops considerably at every density that a new species appears. For comparison we also show  $\gamma$  for the FPS equation, which does not include baryon degrees of freedom beyond nucleons. Indeed, spin up is not found in any normal sequence of the FPS equation, and also does not occur for the EOS with hyperons of Glendenning (Glendenning, N. K. 1997, private communication) because the variation in the adiabatic index is not large enough. The specific details of EOS 2, however, lead to an enhanced effect of hyperon formation on the adiabatic index, which is why we find that spin up is possible for this equation, even for some of the normal neutron star sequences.

Assuming that equations of state which include only nucleons cannot have an effective adiabatic index low enough to allow spin up, a neutron star that spins up without accreting and which does not collapse may serve as important indication of a more complex structure of the core. Spin up

during a pulsar's evolution should in principle be easy to observe, specifically through the breaking index, defined as  $n \equiv \Omega \ddot{\Omega}/(\dot{\Omega})^2$ . The breaking index of observed pulsars is measured to good precision, and is typically found to be 2-3. A pulsar going from spin up to spin down should show a breaking index going to  $-\infty$  at maximum frequency, and then decreases from  $+\infty$  as spin down begins. Glendenning, Pei & Weber (1997) suggested that such behavior of the breaking index may signal the creation of a mixed baryon-quark phase. It is our purpose here to point out that spin up followed by spin down is also a possible (though not a necessary) result of hyperon formation.

Note, however, that spin up occurs for EOS 2 only in high mass stars (rest mass larger than  $1.87 M_{\odot}$ ) which could be uncommon due to selection effects in the pulsar formation mechanism. Furthermore, spin up of stable sequences is only found for very rapidly rotating configurations where nonaxisymmetric instabilities (driven by gravitational radiation) may set in. This further limits the combinations of mass and rotation period that allow spin up in a stable sequence, and could explain why such evolution has not been observed, even if physically possible.

We conclude our discussion of rotational properties and limits of neutron stars in the context of hyperon formation with Fig. 7, which displays the angular velocity versus gravitational mass of constant rest mass sequences for EOS 2 with all types of hyperons. Also plotted in the figure are the known masses and angular velocities for various observed pulsars (see Cook et al. 1994). The horizontal dashed line is a minimum- $\Omega$  limit of  $\Omega = 4032 \text{ sec}^{-1}$  set by PSR 1937+21. The vertical dashed line corresponds to a mass of 1.55  $M_{\odot}$ , which is a suggested lower limit for the Vela pulsar mass (still under debate).

One finds that current combinations of observed pulsar masses and angular velocities do not offer significant constraints on the high density EOS, and, in general, are consistent with hyperon formation (for which EOS 2 may be taken as representative). Note that the maximum angular velocity found for EOS 2 is  $\sim 1.15 \times 10^4 \, {\rm sec}^{-1}$ , well in the range of values of "typical" equations of state. This maximum angular velocity is also in good agreement with the "empirical" formula of Haensel & Zdunik (1989):

$$\Omega_{max} = \chi \left(\frac{M_{max}}{M_{\odot}}\right)^{1/2} \left(\frac{R(M_{max})}{10 \text{ km}}\right)^{-3/2} \text{ sec}^{-1}$$
(5)

where  $M_{max}$  and  $R(M_{max})$  are the gravitational mass and radius of the maximum mass static configuration, respectively. The numerical coefficient  $\chi$  was found by Cook et al. (1994) through a best fit to be  $\chi \approx 7840 \text{ sec}^{-1}$ , when including the supramassive sequences. In general, the softer the EOS, the larger the predicted maximum angular velocity. Since the mistaken measurement from the remnant of SN1987A, there has been much speculation regarding the constraints a 0.5 msec pulsar, if found, would place on the high density EOS. We have not found an EOS where the hyperon induced softening is sufficient to allow a 0.5 msec pulsar, in agreement with other published works.

## **4.4.** Crustal Size and Pulsar Glitches

Pulsar glitch phenomena have been suggested as a probe of neutron star properties (Link, Epstein & Van Riper, 1992). The basic argument is that the interpretation of pulsar glitch phenomena suggests a relatively large crust, which in turn implies a stiff EOS at supernuclear densities, if a pulsar mass greater than 1  $M_{\odot}$  is assumed. Indeed, pulsar glitches are often presented as observational proof that the supernuclear density EOS is stiff (Alpar et al. 1993). However, a stiff EOS

also leads to a large value for the maximum mass, which, as discussed above, is currently difficult to support by observation. We argue here that hyperon formation provides a natural route to combine large crusts *and* a relatively low maximum mass.

Glitches are sudden increases in the rotation frequency of pulsars. The post-glitch behavior of the pulsar indicates a change in the spin-down rate,  $\Delta\dot{\Omega}/\dot{\Omega}$ , ranging from a fraction of a percent (the Crab) to a few percent (the Vela). The generic interpretation of glitches suggests a coupling and decoupling process between different components of the pulsar (Shapiro & Teukolsky 1983). In this event angular momentum is transformed from some weakly coupled component to the bulk of the star, which is strongly coupled to the crust through the magnetic field. This generic interpretation known as the "two-component model", can be shown to predict that

$$\frac{\Delta \dot{\Omega}}{\dot{\Omega}} = \frac{I_c}{I_{tot}} \quad , \tag{6}$$

where  $I_{tot}$  is the total moment of inertia of the pulsar, and  $I_c$  is the moment of inertia of the more rapidly rotating component.

The most successful model suggested so far for pulsar glitches has been the vortex creep theory (Pines & Alpar 1985, Alpar et al. 1993). In this model, the glitches are driven by pinning and unpinning of vortices of the neutron superfluid and the lattice of neutron rich nuclei which coexist in the inner crust of pulsars. Assuming that vortex creep can occur between the density of neutron drip ( $\approx 4 \times 10^{11} \text{ gm/cm}^3$ ) to about half the nuclear saturation density ( $\approx 1.2 \times 10^{14} \text{ gm/cm}^3$ ), where the neutron  $^1S_0$  pairing presumably breaks up and where all nuclei have dissolved to nuclear matter, Eq. (6) can be used to set a lower-limit on the moment of inertia of this part of the star,  $I_{icr}$ . Taking the value obtained from the 1978 Vela glitch  $\Delta\dot{\Omega}/\dot{\Omega} = 0.024$  (Alpar et al. 1993), a significant constraint is placed on the minimal size of the inner crust.

For any EOS, the larger the given gravitational mass, the more compact the neutron star and the larger the fraction of the mass held in the core. Both these effects combine to reduce the fraction of the moment of inertia of the inner crust,  $I_{icr}/I_{tot}$ , as the gravitational mass is increased. Hence, a larger observed value of  $\Delta\dot{\Omega}/\dot{\Omega}$  implies a smaller value for the neutron star gravitational mass in order to satisfy the two-component condition of  $I_{icr}/I_{tot} \geq \Delta\dot{\Omega}/\dot{\Omega}$ . Roughly speaking, a similar combination occurs for a given gravitational mass when comparing a soft EOS to a stiff one, since the softer EOS will yield a more compact star and a smaller crust. We demonstrate this in Fig. 8, which shows the fraction of the moment of inertia carried by the inner crust,  $I_{icr}/I_{tot}$ , as a function of mass for the nuclear matter equations of state presented in Fig. 4, along with EOS 1 and 2 with all hyperon species. The moment of inertia of the neutron star was calculated in the slow-rotation approximation, again following Arnett and Bowers (1977).

All equations show a decrease in  $I_{icr}/I_{tot}$  as a function of the gravitational mass, as discussed above. The key observation, however, is that, with the exception of the very stiff MF model, the inner crust of a 1.4  $M_{\odot}$  neutron star found for nuclear matter matter equations of state is too small to carry a moment of inertia with  $I_{icr} \geq 0.024I_{tot}$ . The equations of state with hyperons are, on the other hand, able to support a large crust in a 1.4  $M_{\odot}$  star, in spite of their maximum masses being relatively low. This is because the crustal size mainly depends on the EOS of the matter just below it, i.e., at  $\rho_B \approx \rho_0$ , while the maximum mass is more sensitive to the EOS at higher densities. Thus, a large crust and a low maximum mass are easily reconciled for any equation of state that is stiff at lower densities, and softens at  $\rho_B \geq 2\rho_0$ .

This may serve to indicate that the EOS should turn from stiff at low densities to soft at higher densities, as speculated in the previous subsections. Again, hyperon formation offers a natural (but not unique) basis for such an EOS to prevail. Once more, we emphasize that this effect regarding crustal size is a generic feature of the inclusion of more species in dense supernuclear matter, and only the finer details will be model dependent.

## 5. Roles of Hyperons in Neutron Star Cooling Rates

In recent years it has been possible to detect X-rays from over twenty pulsars (Ögelman 1995). For a few pulsars, there is strong evidence that actual surface thermal radiation has been detected, while for others only upper limits can be stated. The surface temperature (interpreted from the surface radiation) and the pulsar age (usually estimated through the spin down rate) provide a constraint on the thermal history of the pulsar. Comparison of observation and theoretical models of neutron star cooling may offer a unique indication regarding the composition of the high density matter core, including the presence of new hadronic degrees of freedom.

The implications of hyperon formation for neutron star cooling have been discussed in several recent studies (Prakash et al. 1992, Prakash 1994, Haensel & Gnedin 1994, Schaab et al. 1996). The common theme of these works has been that hyperons provide additional channels for rapid cooling processes, i.e., the direct Urca. Hyperon direct Urca processes, like the nucleon direct Urca, are basically thermal fluctuations of baryons and leptons:

$$B_1 \to B_2 + e + \bar{\nu}_e \; ; \; B_2 + e \to B_1 + \nu_e \; .$$
 (7)

The direct Urca processes allow for large neutrino emissivity, so that rapid core cooling dominates the star's thermal evolution. The direct Urca cooling emissivity,  $\epsilon_{DU}$ , has been estimated as (Prakash et al. 1992)

$$\epsilon_{DU} = 4 \times 10^{27} \left(\frac{x_e \rho_B}{\rho_0}\right)^{1/3} \frac{m_{B_1} m_{B_2}}{m_n^2} R T_9^6 \text{ erg cm}^{-3} \text{s}^{-1} ,$$
 (8)

where  $x_e$  is the electron fraction per baryon,  $m_{B_1}$  and  $m_{B_2}$  are the effective masses of the two participating baryons,  $m_n$  is the neutron mass, and  $T_9$  is the core temperature in units of  $10^9$  °K. R is a weak interaction matrix element factor which is unity for nucleon Urca  $(n \to p + e + \bar{\nu}_e)$ , and ranges between  $\sim 10^{-2}$  for strangeness changing reactions (such as  $\Lambda \to p + e + \bar{\nu}_e$ ) and  $\sim 10^{-1}$  for strangeness conserving reactions which include hyperons (such as  $\Sigma^- \to \Lambda + e + \bar{\nu}$ ); see the review by Prakash (1994) for details.

If neutron stars cool through direct Urca processes indefinitely, their temperature should drop so rapidly that the surface temperatures (typically  $10^{-2}$  of the core temperature) would be undetectable within less than 100 years of the star's birth (Lattimer et al. 1994). Observation seems to suggest otherwise, indicating that direct Urca processes are suppressed in the core through most of the star's thermal evolution, so that a significant surface temperature can be detected even at pulsar ages of  $10^3 - 10^5$  years. If the direct Urca is indeed suppressed, then cooling proceeds through less efficient processes, most of which have emissivities  $\sim T_9^8$  (with various numerical coefficients (Maxwell 1987)). Calculations of neutron star thermal evolutions in which slower cooling processes dominate do find that the surface temperature remains rather large for  $\sim 10^5$  years, until crust photon emission takes over as the dominant cooling process.

Direct Urca processes may be suppressed by two main mechanisms: absolute suppression if energy and momentum cannot be conserved, and partial suppression if the participating baryons pair to a superfluid state. The presence of hyperons in neutron star cores has implications on both issues, as discussed below.

### **5.1.** Threshold Concentrations

Due to the extreme degeneracy of fermions in neutron star cores, direct Urca reactions take place only with baryons and leptons on their respective Fermi surfaces. Imposing energy and momentum conservation (and assuming a negligible neutrino energy:  $E_{\nu} \approx k_B T$ ), leads to a combination of the conditions:

$$\mu_{B_1} = \mu_{B_2} + \mu_e \quad ; \quad p_F(B_1) \le p_F(B_2) + p_F(e) \quad ,$$
 (9)

 $p_F(X)$  being the Fermi momenta of species X. The first condition simply imposes chemical equilibrium which is fulfilled inherently (Eq. (2)), and the second is the "triangle inequality", which must be fulfilled for all cyclic permutations of the  $B_1, B_2$  and e. For Fermions  $p_F = (3\pi^2 x \rho_B)^{1/3}$ , so that the second condition of Eq. (9) becomes  $x_1^{1/3} \leq x_2^{1/3} + x_e^{1/3}$  (again, along with all cyclic permutations).

According to the momentum-conservation condition above, direct Urca processes may take place only if the relative fractions of the two baryon species are not too different from one another, and from the electron fraction as well. The fractions required set threshold conditions for the existence of direct Urca processes, which are otherwise completely extinct. For nuclear matter in beta-equilibrium it has been shown that the large neutron excess requires a threshold proton fraction of at least  $x_{pc} \ge 11-15\%$  (Prakash et al. 1992) to allow the nucleon direct Urca process to take place. Whether or not a large enough proton fraction exists in the cores of neutron stars depends on the specifics of the nuclear matter EOS. Once hyperons appear in the matter, threshold concentrations are easier to meet for all types of direct Urca processes. First, the threshold concentrations for some hyperon processes with protons or other hyperons are inherently low - typically on the order of 0.01 - since their fractions are initially similar (Prakash 1994). Second, since hyperon formation is followed by an increase of the proton fraction and a reduction of the neutron fraction, the threshold concentrations for neutron related Urca processes are also easier to fulfill, including nucleon direct Urca  $(x_p/x_n \ge 0.1)$ .

Direct Urca processes will become prohibited if the electron fraction is too small to allow for momentum conservation (i.e., the triangle inequalities cannot be fulfilled). However, for typical equilibrium compositions with hyperons, this happens only when the electron fraction drops below about 0.5%, which does not occur at the central density of a 1.4  $M_{\odot}$  star as found with practically all published equations of state. The small lepton fraction induced by hyperon formation will also reduce the direct Urca emissivities through the  $x_e$  dependence in Eq. (8). However, even for  $x_e \approx 0.1\%$  this suppression is only by a factor of a few (and the effect on the cooling rate will be somewhat balanced by a reduction of the star's heat capacity). Hence, the composition of a hyperon rich core should allow for at least most direct Urca processes to dominate in typical neutron stars.

### **5.2.** Superfluidity

In view of the lenient conditions for hyperon direct Urca reactions, theoretical models of neutron star thermal evolution find that stars with hyperons will cool very rapidly (Haensel & Gnedin 1994, Schaab et al. 1996). However, these analyses assumed that all hyperons are in a normal, rather than a superfluid state. Here we wish to call attention to the implications of a recent estimate of hyperon pairing gaps.

Baryon superfluidity may have various consequences on neutron star properties including a significant moderation of cooling processes. If the baryons on the Fermi surface couple to superfluid pairs with a gap energy of  $\Delta$ , the direct Urca emissivity is reduced by a factor of  $\sim \exp(-\Delta/k_BT)$ , since an energy of  $\Delta$  is first required to break up the superfluid pair. Nucleon pairing in neutron stars has received much attention, and for the last two decades it has been widely accepted that nucleons can couple to superfluid pairs in neutron stars. The commonly accepted picture (Shapiro & Teukolsky 1983) is that neutrons in the inner crust couple to a  $^1S_0$  superfluid, while in the core the neutrons couple to a  $^3P_2$  superfluid (due to their high Fermi momenta) and the protons couple to a  $^1S_0$  superconductor. Estimates of the gap energies have proven to be model dependent, but core gap energies are typically found to be in the range 0.1 to 1 MeV. The existence of baryon pairing is expected when the temperature drops below the critical temperature, which is  $\sim 0.57\Delta/k_B$  for S—wave pairing and  $\sim 0.12\Delta/k_B$  for P—wave pairing. Neutron stars are expected to cool below the critical temperatures for nucleon pairing within days after their birth, and so nucleon pairing is conventionally assumed to be present in neutron star cores, with a significant impact on nucleon direct Urca emissivity (Lattimer et al. 1994, Page 1995, Schaab et al. 1997).

Until recently, quantitative estimates of pairing of other baryon species have not been performed due to lack of relevant experimental data. In a recent work, Balberg & Barnea (1998) used an analysis of doubly strange hypernuclei in a first attempt to determine pairing gaps for  $\Lambda$  hyperons in a neutron star matter background. The  $\Lambda$  hyperons were found to couple in a  $^1S_0$  superfluid, with a gap energy of a few tenths of an MeV. S-wave pairing is expected for  $\Lambda$  Fermi momenta up to about 1.3 fm<sup>-1</sup>, very much like the corresponding value for protons in a neutron matter background (Elgarøy et al. 1996). These results imply that for typical models of hyperon formation in neutron stars, a  $\Lambda$   $^1S_0$  superfluid will exist between the threshold baryon density for  $\Lambda$  formation and the baryon density where the  $\Lambda$  fraction reaches 15–20%. While this result is based on limited data from double hypernuclei (i.e., nuclear matter background at normal nuclear density), the basic prediction of a  $\Lambda$  superfluid is not surprising, in view of the general similarity of  $\Lambda$  –  $\Lambda$  and nucleon—nucleon interactions. Further work is clearly necessary, and estimation of gap energies for other hyperon species is also required (including possible anisotropic pairing modes), but in general, it seems prudent not only to allow for hyperon formation in neutron stars, but also to include hyperon superfluidity.

A full treatment of neutron star cooling with superfluid hyperons is beyond the scope of this study, and is reported to another work (Schaab, Balberg, & Schaffner-Bielich 1998). We point out that for suppression of all direct Urca processes, it is sufficient that only the neutral baryons, e.g., n,  $\Lambda$  and  $\Sigma^0$  (or n,  $\Lambda$  and  $\Xi^0$ , if  $\Sigma$ 's are absent), couple to a superfluid state: charged baryons will be deprived of partners for the direct Urca processes. Furthermore, at central densities typical of a 1.4  $M_{\odot}$  neutron star (in most equations of state), fractions of neutral hyperons other than the  $\Lambda$  are very small, so  $\Lambda$  and neutron superfluidity are sufficient to significantly moderate all relevant

direct Urca processes. The core temperature should then saturate according to the lower of the neutron  $^3P_2$  and the  $\Lambda$   $^1S_0$  critical temperatures, with the surface temperature declining very slowly for  $10^4 - 10^5$  years. Correspondingly, hyperon formation can indeed be compatible with observed thermal emission from pulsars.

## 6. Roles of Hyperons in Phase Transitions

We now return to possible phase transitions of high density matter in the cores of neutron stars. There are two such transitions which may occur in the matter: the formation of an S-wave meson condensate, and deconfinement of baryons into quarks. Both types of transitions have been the subject of intensive study, but whether or not one (or both) of them can actually take place in cold, beta-equilibrated supernuclear density matter remains an open question. This is mainly because the details of the transitions are dependent on physical values (i.e., meson effective masses and quark matter physics) which are currently unattainable by experiment, leaving uncertainties that are too large to significantly constrain predictions.

While these phase transitions are of obvious interest from the particle physics point of view, they also have astrophysical implications through their possible effects on neutron star properties (mass radii relations, cooling rates, etc.). For our discussion here it is important that both types of transitions offer alternative hadronic degrees of freedom to hyperon formation. Indeed, both meson condensation and deconfinement have been demonstrated to soften the equation of state and cause deleptonization (offering negatively charged hadrons or quarks to replace the leptons), therefore leading to most of the effects discussed in previous sections (Prakash et al. 1997). Furthermore, meson condensation and baryon deconfinement offer potential competition to hyperon formation, since they too lower the energy per baryon of the matter, thereby decreasing the nucleon chemical potentials. In this section we examine what influence the presence of hyperons in the cores of neutron stars can have on meson condensation and baryon deconfinement.

### **6.1.** Meson Condensates

Mesons may form freely in baryonic matter since they do not obey number conservation. At zero temperature, a nonzero meson density naturally takes the form of a Bose condensate, where the required energy for meson accumulation is only the meson ground state energy which may be identified through the meson effective mass. Thus, the candidates considered most likely for condensation in neutron star matter are the lightest mesons - the pion and the kaon.

At low densities (including in nuclei), the available energy is insufficient to maintain a nonzero mesonic density and mesons serve only as carriers of the baryonic interactions. At higher densities the available energy in the strong interactions increases, and at some finite density mesons may begin to condense.

Since the baryonic content of the matter has a net positive charge, the best candidates for condensation are the negatively charged mesons. The relevant meson creating reactions are:  $B_1 \to B_2 + \pi^-$  or  $B_1 \to B_2 + K^-$  (with additional particles participating in order to conserve momentum). The fundamental point is that these processes are equivalent to the lepton-related reactions (Eq. (1)), so that the mesons basically compete with the charged leptons. Since neutrinos

and anti-neutrinos are assumed to have zero chemical potential, the basic condition for negatively charged meson condensation is

$$m_{M^-}^* = \mu_e \quad , \tag{10}$$

where  $M^-$  denotes the  $\pi^-$  or  $K^-$ , and  $m^*$  denotes the meson effective mass, which may differ from the bare mass due to medium effects. Note that for neutral mesons the condition for condensation is  $m_{M^0}^* = 0$  and for positively charged mesons it is even  $m_{M^+}^* = -\mu_e$ .

The condition in Eq. (10) implies that hyperon formation has a fundamental influence over the likelihood of meson condensation in neutron star matter. This can be seen explicitly in Fig. 9, where the electron chemical potential is plotted as a function of baryon density for the equilibrium compositions found with equations of state 1 and 2 presented above. The plots correspond to the nuclear matter case (identical in both cases, since they have a common nuclear symmetry term), matter with all types of hyperons, and matter with  $\Lambda$ 's and  $\Xi$ 's but no  $\Sigma$ 's.

The qualitative difference between nuclear matter and matter with hyperons is explicit, and is an obvious result of the deleptonization hyperons induce in the matter. For nuclear matter the electron fraction gradually rises for larger densities, and the electron chemical potential reaches 300 MeV and more. On the other hand, the onset of hyperon accumulation is followed by a drop in the electron fraction, and a corresponding reduction in the electron chemical potentials. This is especially pronounced when negatively charged hyperons appear. The electron chemical potential typically reaches a maximum value which is somewhat model dependent at about 200 MeV, and at very high densities drops to even less than 100 MeV. Since limiting the electron chemical potential is an immediate consequence of hyperon formation (see also Glendenning 1996), this suggests another general result: meson condensation is less likely in matter with hyperons than in nuclear matter.

Whether or not the deleptonization is sufficient to deny meson condensation also depends on the values of the meson effective masses, which are poorly known at present. Evaluating the meson effective mass as a function of the baryon density and composition requires the self-consistent inclusion of the meson fields in the Lagrangian, which we do not follow here.

We do note that modern estimates of the  $\pi$ -nucleon interaction find that the  $\pi$  effective mass is expected to grow with respect to the bare value of  $\approx 140$  MeV due to the strength of the nucleon particle-hole interaction (Brown et al. 1988, Baym 1991; see also Waas, Brockmann & Weise 1997, for a recent estimate). Hence, even though the  $\pi^-$  was considered a natural candidate for condensation in many early works, most current studies agree that such condensation is unlikely, even in nuclear matter. Hyperon formation will have an indirect effect on the likelihood of condensation of other pion species as well, since it reduces the total energy per baryon of the matter. However, this effect cannot be estimated quantitatively in the context of the models used in this work. In principle, repulsive  $\pi N\Delta$  coupling should suppress condensation of other pion species as well (Baym 1991). But it should be noted that variational models performed with Argonne three-body forces (Wiringa et al. 1988, Akmal et al. 1998) find that strong tensor correlations which imply neutral pion condensation appear in nuclear matter at very low densities of about 0.2 fm<sup>-3</sup>.

Unlike the pion, analysis of  $K^-$  atomic data (e.g., Friedman, Batty & Gal 1994) suggests an attractive  $K^-$ -nucleon potential which reduces the bare mass of about 500 MeV by a sizable fraction. Indeed,  $K^-$  condensation in neutron star matter has become an active subject of investigation since first suggested by Kaplan and Nelson (1986). Some studies of  $K^-$  condensation in nuclear matter have found a threshold condensation density as low as  $3-4\rho_0$  (Brown et al. 1994, Pandharipande,

Pethick & Thorsson, 1995). However, an effective  $K^-$  mass as low as 200 MeV at a density of  $2\rho_0$  seems unattainable in present studies (see also Schaffner et al. 1994). In view of the analysis displayed in Fig. 9, this implies that hyperons will appear in nuclear matter prior to the onset of  $K^-$  condensation, and thus delay the condensation to higher densities. This observation is indeed supported by the results of two recent studies (Knorren et al. 1995, Schaffner & Mishustin 1996), which examined  $K^-$  condensation along with hyperon formation. Both find that hyperons appear before the  $K^-$  can condense in nuclear matter, and that condensation in matter with hyperons is then delayed to very large densities ( $\geq 8\rho_0$ ) or even completely suppressed.

Clearly, should meson condensation occur at lower densities than hyperon formation, it is the latter that will be delayed, but this alternative seems less likely in view of most current works. Assuming it is hyperon formation that precedes, it will increase the threshold density for meson condensation, and this is once again a general feature of allowing for hyperon formation in neutron stars.

# **6.2.** Baryon Deconfinement

The possibility of a phase transition of high density baryonic matter into quark matter through baryon deconfinement has received much attention both in the context of neutron stars and in heavy ion physics. Intuitively, it seems inevitable that at large enough densities the quarks will no longer retain their arrangement as baryons, but rather deconfine into larger "bags" of quarks, and eventually into quark matter. However, present theoretical limits and uncertainties in the modeling of QCD prevent a comprehensive analysis of deconfinement physics. Current studies rely on simplified models, and published results and conclusions prove to be highly model dependent. Nonetheless, as we show below, the presence of hyperons does have a general effect on the phase transition between baryonic and quark matter.

Baryon deconfinement in high density matter is expected to proceed gradually with increasing density through a continuous mixed phase with various spatial combinations of the two phases. This is analogous to the transition from nuclei to nuclear matter in the inner crusts of neutron stars. The ground state at each density is achieved by arranging the composition, density and shape of each phase, including long range ordering enforced by the Coulomb interaction. This character of the transition from baryon matter to quark matter was pointed out by Glendenning (1992, see Glendenning 1996 for a review), and is a natural consequence of the presence of two conserved charges - baryon number and electric charge. Pressure varies continuously over the density range of the transition, rather than remaining constant as in a "standard phase transition". A neutron star which includes a mixed phase (and possibly, at very high densities, a pure quark phase) is often referred to as a "hybrid star".

It is important to note that the conditions for the onset of deconfinement differ considerably from the conditions for equilibrium of the two phases. The key factor is the difference in the strangeness fraction of the equilibrium compositions of the two phases. In the quark phase the difference between the mass of the strange quark and those of the up and down quarks is significantly lower than the Fermi energies of the quarks. The equilibrium quark composition should therefore hold almost equal fractions of the three flavors, with a strangeness fraction per baryon of almost unity. In the baryonic phase an overall strangeness fraction of unity can be reached only at very high densities, when the baryon masses no longer dominate the values of the chemical potentials.

Once a stable quark matter phase is created, it reaches its equilibrium composition through weak decays, regardless of the initial baryon composition. The initial deconfinement process, however, must take place through the strong interaction, which conserves flavor. The minimum energy state a quark phase component can achieve through deconfinement will not be its ground state, but only the lowest energy state with the available underlying quark composition of the baryons. It is therefore straightforward that when the baryonic matter includes a finite strangeness fraction (i.e., hyperons are present), the energy a quark phase component can achieve through deconfinement will be lower than for a two-flavor quark phase created by deconfinement of pure nucleon matter. The presence of hyperons lowers the energy per baryon with respect to nuclear matter in the baryonic phase as well, but the effect of a finite strangeness fraction in the quark phase is significantly larger. The threshold for deconfinement of matter with hyperons should thus be lower than for nuclear matter.

We demonstrate this qualitative description with a crude analysis for the deconfinement threshold, as follows: assume that baryonic matter deconfines as a bulk, where baryons at a given density  $\rho_B$  deconfine spontaneously to quark matter of identical density and quark composition. Such deconfinement will proceed if the energy per baryon in the quark phase is equal to (or less than) that in the baryonic phase. Figure 10 compares the energy per baryon,  $E/A = \varepsilon_B/\rho_B$ , as a function of the density of the equilibrium baryon compositions of EOS 1 with the energy per baryon of quark matter of identical composition and density. The properties of the quark phases in each case are calculated with simple MIT bag model parameterizations, where B is the bag constant (in MeV/fm<sup>3</sup>) and  $\alpha_c$  is the strong interaction coupling constant (see chapter 8 in Glendenning 1996).

The baryon density of deconfinement corresponds to the crossover between the baryonic matter and quark matter curves. The effect of finite strangeness on the energy per baryon is much more pronounced in the quark phase, resulting in an observable decrease of the energy per baryon when a new hyperon species appears in the matter (i.e., where the strangeness fraction increases rapidly with density). The density of deconfinement for any given quark matter model is then lower for matter with hyperons than for nuclear matter.

The specific value of the deconfinement density is strongly dependent on the values of the bag model constants. Since the values used in the calculations are arbitrary, emphasis is placed on the fundamental reduction in the threshold for deconfinement in the presence of hyperons. Once again, this is a general feature of allowing hyperons to appear in the matter. We also find a lower deconfinement density for other high density equations of state (when comparing matter with hyperons and nuclear matter), and that it is independent of the specific choice of quark bag model constants.

While the assumption that the baryon-quark phase transition proceeds through bulk deconfinement is a crude one, it actually provides an upper limit for the deconfinement threshold. The alternative to bulk deconfinement is nucleation of quark bubbles in the baryonic background, when only some of the baryons deconfine. For a quark bubble to survive it must maintain thermodynamic and chemical equilibrium of strong interactions with the baryon background while the net flavor of all of the matter must still be conserved. Unlike the bulk deconfinement scenario, quark bubbles can compress or expand to have a different density than the surrounding medium. They can also maintain a composition different from the original baryons by controlling the fractions of baryon

species which deconfine. This implies that bubble nucleation has more degrees of freedom than bulk deconfinement, and the possibility for the quark bubbles to have a larger strangeness fraction than the baryon background is especially helpful for bubble formation. This qualitative argument suggest both that the threshold density for deconfinement is lower for bubble nucleation than for bulk deconfinement, and that the impact of strangeness being present should be even more pronounced in this case. Calculations of bubble nucleation are, however, highly model dependent, since additional factors such as the bag surface tension must be included (see, e.g., Olesen & Madsen 1994), and we confine ourselves to these qualitative remarks.

Finally, it is interesting to note that in equilibrium, the presence of hyperons is expected to increase the minimal baryon density in which a mixed phase can exist with respect to nuclear matter (Prakash et al. 1997). Hyperon formation reduces the energy per baryon, and at any total baryon density the quark component of the mixed phase always occupies less volume and holds less baryon number when equilibrated with a baryonic phase with hyperons than when equilibrated with nucleons. However, since the mixed phase can only appear following the initial deconfinement, hyperon formation does not suppress deconfinement, but rather enhances it, as is evident from Fig. 10 and the discussion above. Furthermore, since hyperons soften the equation of state, a larger central baryon density is required to support a star of given mass than for nuclear matter. We conclude that the likelihood of deconfinement and creation of a mixed phase in neutron stars is increased by the appearance of hyperons with respect to nuclear matter. This likelihood is difficult to quantify, since it is strongly dependent on the quark matter equation of state, which may delay deconfinement to extremely high densities, or even forbid it from occurring in the density range relevant to neutron star cores (in the context of the bag model, this is naturally achieved by increasing B). Nonetheless, these general implications of hyperon formation are, yet again, model independent.

## 7. Conclusions and Discussion

Various recent studies of hyperon formation in neutron stars share a consensus, that hyperons will appear in the cores of neutron stars at a density of about  $2\rho_0$ . This consensus is a direct consequence of the common basis used in these works for describing the hyperon-nucleon and hyperon-hyperon interactions, as deduced from hypernuclei experiments. The qualitative principle which arises from these experiments is that hyperon related interactions are similar both in character and in order of magnitude to the nucleon-related interactions. It is thus reasonable for the fundamental similarity of nucleons and hyperons to be manifest at higher densities, where the typical energy scales are of the order of the mass differences between the different species. In this study we concentrate on the effects hyperon formation may have on the global properties of neutron stars. We discuss the implications of the presence of hyperons in the cores of neutron stars for the high density equation of state, for cooling reactions, and for phase transitions which could be possible in high density matter.

The fundamental effect of hyperon formation on high density matter is the softening of the equation of state with respect to the equation found for nuclear matter when using otherwise identical assumptions regarding the strong interactions. This effect is found in all the works which include hyperons in high density matter, and simply reflects that a larger number of baryonic

degrees of freedom relieves some of the Fermi pressure of the nucleons. We also demonstrate a more subtle effect, where the rate at which the strong interaction potential energy density rises as a function baryonic density (due to repulsive short range forces) determines both the stiffness of the nuclear matter equation of state and the rate of hyperon accumulation. These two processes tend to balance one another in terms of the overall equation of state, and so hyperons induce a "pressure control" mechanism in the matter, in the sense that the equations of state for matter with hyperons are limited to a narrower range than nuclear matter equations of state. The clearest manifestation of the "pressure control" mechanism is that the maximum neutron star masses found for equations of state with hyperons are limited to a rather narrow range - in this work 1.5–1.8  $M_{\odot}$  - much smaller than the range found for nuclear matter equations. A narrow range for the value of the maximum mass is in good agreement with published works, and we emphasize that it is a fundamental consequence of hyperon formation in neutron stars, while specific details of the modeled interactions are only of secondary importance.

Hyperon formation provides a natural route to combine a stiff equation of state at a density of  $\rho_B \sim \rho_0$  and a softer equation at higher densities  $\rho_B \geq 2\rho_0$ . Such a combination could make a large mass neutron star significantly more compact than a 1.4  $M_{\odot}$  star, and can even enable some specific configurations to undergo a spin-up period during their rotational evolution. Current observations do not provide positive or negative indication regarding such a combination in the equation of state, but we do point out that it can also reconcile a large neutron star crust, implied from pulsar glitch phenomena, with a low to intermediate maximum mass. This is in contrast to the argument made regarding nuclear equations of state, claiming the glitches indicate a stiff equation at high densities.

Once hyperons are included, the baryon composition of neutron star cores provides the necessary concentration thresholds for direct Urca neutrino emitting processes. This can lead to rapid cooling rates of neutron stars, but the actual cooling rates may be severely moderated if the baryons couple to superfluid pairs. While nucleon superfluidity has been discussed extensively in the past, we point out that hyperons should also be expected to be in a superfluid state, with gap energies in the same order of magnitude. Hence, hyperon formation can be consistent with observed cooling rates.

Both meson condensation and baryon deconfinement offer alternative degrees of freedom to hyperon formation in high density matter. The threshold densities for both types of phase transitions are difficult to constrain, due to large uncertainties involved. However, current estimates of the properties of high density matter suggest that hyperon formation will precede meson condensation and deconfinement. We show that if indeed hyperons appear first in the matter they affect the likelihood of both these transitions. Meson condensation is suppressed, since hyperons induce deleptonization, thus lowering the lepton chemical potential with which the mesons compete. On the other hand, the finite strangeness fraction allows the baryons to deconfine into a lower energy quark matter state, making deconfinement more favorable for any given quark matter physics. Both these trends are opposite than those expected in high density nuclear matter, which has a large lepton fraction and is composed of only strangeless quarks.

We emphasize again that all these results are basically general features of matter with multiple baryon species. Most of the specific quantitative values are dependent on the details of the modeling of the strong interaction, but the qualitative results discussed here should prevail as long as the general nature of these models is similar. It should be borne in mind that while the extrapolation of these interactions from hypernuclei data seems reasonable, large uncertainties still remain. If some of the hyperon-nucleon interactions are critically different than those assumed here, the qualitative trends can change through suppressing the formation of some baryon species.

Unfortunately, the current status of observations of neutron stars does not provide any significant constraints on the properties of high density matter. Specific indications for the presence or absence of hyperons are naturally unavailable as well. Clearly, any further measurements of masses, radii and rotation frequencies will be extremely valuable for constraining the high density equation of state, especially if unusual values (such as a large mass or a rapidly rotating star) will be observed. Correlations between these different quantities for any given object are also important, and the newly discovered Quasi-Periodic-Oscillations in kilohertz emission in some X-ray binaries may offer potential in this regard.

Unique features of neutron stars, if observed, may also provide some indication regarding the physics of high density matter. If several hyperon species do form in the core, the core could be composed of multiple superfluids, including some negatively charged superconductors. Such a composition might have effects on both the rotational properties and the magnetic evolution of the star. Further differences with respect to nuclear matter might be found due to the lower density (by more than an order of magnitude) of the normal (not-superconducting) lepton component, in particular through the magnetic field evolution.

Needless to say, additional experimental data from hypernuclei will be useful in establishing the foundations of high density matter models. This is especially relevant to the hyperon-nucleon interactions, for which relevant systems are more likely to be produced in current accelerators than for hyperon-hyperon interactions.

Finally, we recall that the properties of high density matter may have important consequences in several related astrophysical processes. Of these, the evolution of a newly born neutron star has received extensive attention in recent years (see, e.g., Keil & Janka 1995, Prakash et al. 1997). A unique qualitative feature in this regard is that matter with hyperons (and also with other negatively charged hadrons or quarks) will support a smaller maximum mass after neutrinos diffuse from the newly born core than while neutrinos are still trapped. Once lepton number in the matter is allowed to decrease, more hadronic degrees of freedom can be exploited which will soften the equation of state. For nuclear matter the opposite occurs, since deleptonization leads to a larger neutron-proton asymmetry, which stiffens the equation of state. The maximum mass of a star with hyperons in the core is found to be larger when neutrinos are still trapped than after deleptonization. implying a mass range for which a newly born neutron star is meta-stable. Hyperon formation may thus play a role in creating another route for the formation of low mass black holes in type II supernova, with neutrino emission setting the time scale for the collapse (10-15 seconds). Such a scenario is especially appealing in view of the neutrino measurements from SN1987A (Ellis, Lattimer & Prakash 1996), in which no neutron star has been found. If a future nearby supernova will provide finer details regarding the emitted lepton number, neutrino energy content and time structure, valuable information may be inferred regarding high density matter and its composition, and hyperon formation in particular.

We are grateful to Avraham Gal, Zalman Barkat and Christoph Schaab for valuable advice and suggestions. This research was partially supported by the U.S.-Israel Binational Science Foundation

grant 94-68.

## A. The Effective Equation of State

The formalism of the effective equation of state discussed in this work was presented by Balberg & Gal (1997, to which the reader is referred for detail). This equation is basically a generalization of the Lattimer-Swesty equation of state for nuclear matter (Lattimer & Swesty 1991), which is commonly used in hydrodynamical simulations. An effective equation of state does not presume to describe the underlying physics of the strong interactions, but does allow for conducting extensive parameter surveys (including finite temperatures). The effective equation was shown to reproduce the main results of field theoretical models in terms of the equilibrium compositions and the thermodynamic properties of the high density matter.

The core of the effective EOS is an adjustable baryon-baryon potential, which models the strong interaction and provides the quantitative description of the potential energy density of high density matter. This energy density is added to the kinetic energy and mass densities of the baryons, and to the kinetic energy and mass densities of the leptons, which are taken to be noninteracting (as is commonly assumed).

The baryon-baryon interactions among the various species are described by assuming local density-dependent potentials. These potentials are constructed to reproduce the basic features of the strong interactions, i.e., long-range attraction and short range repulsion, and - in some cases - charge dependence, compatible with isospin invariance. The potential felt by a single baryon of species y in bulk matter of baryon species x with number density  $\rho_x$  is then given in the form

$$V_y(\rho_x) = a_{xy}\rho_x + b_{xy}t_xt_y\rho_x + c_{xy}\rho_x^{\gamma_{xy}} + w\rho_x^{\theta} . \tag{A1}$$

The first term yields attraction ( $a_{xy}$  negative), the third and fourth terms yield repulsion ( $c_{xy}$  and w positive, supposedly introducing multibody interactions), and the second (symmetry) term introduces the charge dependence through a charge (isospin) t. Both  $\gamma_{xy}$  and  $\theta$  are greater than unity so that repulsion will dominate at high densities (short ranges). The fourth term included here was found to preempt some numerical problems which arose when a single repulsive term was used (Balberg & Gal 1997). This term is assumed to represent universal short range interactions, thus setting w and  $\theta$  to be independent of the baryon species involved. The values of the coefficients and exponents are chosen to reproduce experimental data and accepted theoretical results regarding the baryon-baryon interactions.

The local potential for a single baryon in a bulk of other baryons may be extrapolated into the potential energy density of bulk matter with a total density  $\rho$  that includes both types of baryons. This is done by folding  $V_y(\rho_x)$  with the partial density  $\rho_y$ , and vice versa  $(V_x(\rho_y))$  with  $\rho_x$ , combined with weight factors (avoiding double counting of each interaction). For simplicity we assume that all baryon-baryon interactions have a common value of  $\gamma$  (further generalization is, of course, possible), and follow the common assumption of universal hyperon couplings (denoted below as  $a_{YY}$  and  $c_{YY}$ ). The final expression for the potential energy density of baryonic matter with a baryon density  $\rho$  is then:

$$\varepsilon_{pot}(\rho) = \frac{1}{2} \left[ a_{NN} N^2 \rho^2 + b_{NN} (n-z)^2 \rho^2 + c_{NN} N^{\gamma+1} \rho^{\gamma+1} \right]$$

$$+ a_{\Lambda N} N \Lambda \rho^2 + c_{\Lambda N} \left( \frac{N}{N+\Lambda} N^{\gamma} \Lambda + \frac{\Lambda}{N+\Lambda} \Lambda^{\gamma} N \right) \rho^{\gamma+1}$$
(A2)

$$\begin{split} &+\frac{1}{2}\left[a_{\Lambda\Lambda}\Lambda^{2}\rho^{2}+c_{YY}\Lambda^{\gamma+1}\rho^{\gamma+1}+a_{YY}\Xi^{2}\rho^{2}+b_{\Xi\Xi}(\Xi^{-}-\Xi^{0})^{2}\rho^{2}+c_{YY}\Xi^{\gamma+1}\rho^{\gamma+1}\right]\\ &+a_{\Xi N}N\Xi\rho^{2}+b_{\Xi N}(n-z)(\Xi^{-}-\Xi^{0})\rho^{2}+c_{\Xi N}\left(\frac{N}{N+\Xi}N^{\gamma}\Xi+\frac{\Xi}{N+\Xi}\Xi^{\gamma}N\right)\rho^{\gamma+1}\\ &+a_{YY}\Xi\Lambda\rho^{2}+c_{YY}\left(\frac{\Lambda}{\Xi+\Lambda}\Lambda^{\gamma}\Xi+\frac{\Xi}{\Xi+\Lambda}\Xi^{\gamma}\Lambda\right)\rho^{\gamma+1}\\ &+a_{\Sigma N}N\Sigma\rho^{2}+b_{\Sigma N}(n-z)(\Sigma^{-}-\Sigma^{+})\rho^{2}+c_{\Sigma N}\left(\frac{N}{N+\Sigma}N^{\gamma}\Sigma+\frac{\Sigma}{N+\Sigma}\Sigma^{\gamma}N\right)\rho^{\gamma+1}\\ &+a_{YY}\Sigma\Lambda\rho^{2}+c_{YY}\left(\frac{\Sigma}{\Sigma+\Lambda}\Sigma^{\gamma}\Lambda+\frac{\Lambda}{\Sigma+\Lambda}\Lambda^{\gamma}\Sigma\right)\rho^{\gamma+1}\\ &+a_{YY}\Sigma\Xi\rho^{2}+b_{\Sigma\Xi}(\Xi^{-}-\Xi^{0})(\Sigma^{-}-\Sigma^{+})\rho^{2}+c_{YY}\left(\frac{\Xi}{\Xi+\Sigma}\Xi^{\gamma}\Sigma+\frac{\Sigma}{\Xi+\Sigma}\Sigma^{\gamma}\Xi\right)\rho^{\gamma+1}\\ &+\frac{1}{2}\left[a_{YY}\Sigma^{2}\rho^{2}+b_{\Sigma\Sigma}(\Sigma^{-}-\Sigma^{+})^{2}\rho^{2}+c_{YY}\Sigma^{\gamma+1}\rho^{\gamma+1}\right]+\frac{1}{2}w\rho^{\theta+1}\;, \end{split}$$

where for each species  $x = \rho_x/\rho$  and introducing the shortened notation N = n + z;  $\Xi = \Xi^0 + \Xi^-$ ;  $\Sigma = \Sigma^+ + \Sigma^0 + \Sigma^-$ . In equation (A2) it is assumed that isospin (symmetry) forces vanish for the  $\Lambda$  and  $\Sigma^0$ , which have a zero isospin projection  $(I_3 = 0)$ .

Current experimental data are insufficient to constrain all the presented coefficients, especially those corresponding to the short range interactions. Once the shape of these interactions is assumed (by setting the value of w and  $\theta$ ), the rest of the coefficients can be determined by fitting them to reproduce the properties of nuclei and hypernuclei. In this work two sets of coefficients were used, denoted models 1 and 2. These models differ mainly in their density dependence (the values of  $\gamma$  and  $\theta$ ), and correspondingly reflect two values for the incompressibility of symmetric nuclear matter at  $\rho_N = \rho_0$ : (1) K = 240 MeV, which is a "standard" value used for high density matter, and (2) K = 320 MeV which implies a stiff EOS. The values of the coefficients in both equations are given in Tab. 2. In the variation where  $\Sigma$  hyperons are excluded from the matter, the coefficients of the  $\Sigma$  related interactions are ignored.

Since the effective EOS has no means of consistently combining relativistic and medium effects, the masses are set to be equal to the bare ones. This is a somewhat crude approximation, since field theoretical models suggest an effective baryon mass lower than the bare one, although the values of the coefficients in the potential energy expression can compensate in part for this approximation. Correspondingly, the baryons are treated as non-relativistic. We note that the equations do reach the causality limit,  $dP/d\varepsilon = c^2$ , but in both cases this occurs at densities which correspond to neutron star masses slightly higher than the maximum static mass.

Approximating neutron star matter to have zero temperature, the kinetic energy and mass density terms for the baryons are, respectively:

$$\varepsilon_{kin}(\{x_i\}, \rho_B) = \sum_i \frac{p_F^2(x_i)}{2m_i} \quad \varepsilon_{mass}(\{x_i\}, \rho_B) = \sum_i x_i \rho_B m_i \quad , \tag{A3}$$

where  $p_F(x_i) = \hbar c (3\pi^2 x_i \rho_B)^{1/3}$  is the Fermi momenta of the baryons. The lepton relativistic energy densities (dependent on the lepton fraction and the total density) are added as well, yielding the final EOS,  $\varepsilon(\{x_i, x_l\}, \rho_B)$ .

#### REFERENCES

Akmal, A., Pandharipande, V. R., & Ravenhall, D. G. 1998, Phys. Rev. C, 58, 1804

Alpar, M. A., Chau, H. F., Cheng, K. S., & Pines, D. 1993 ApJ, 409, 345

Ambartsumyan, V. A., & Saakyan, G. S. 1960, Soviet Ast., 4, 187

Arnett, W. D., & Bowers, R. L. 1977, ApJS, 33, 415

Balberg, S., & Gal, A. 1997, Nucl. Phys. A, 625, 435

Balberg, S., & Barnea, N. 1998, Phys. Rev. C57, 409

Batty, C. J., Friedman E., & Gal A. 1994, Phys. Lett. 335, 273

Baym, G. 1991, in Neutron Stars, Theory and Observation, ed. J. Ventura & D. Pines (Dordrecht: Kluwer), 25

Baym, G., Bethe, H. A., & Pethick, C. J. 1971, Nucl. Phys. A, 175, 225

Baym, G., Pethick, C. J., & Sutherland, P. 1971, ApJ, 170, 299

Bethe, H. E., & Brown, G. E. 1995, ApJ, 445, L29

Bethe, H. E., & Johnson, M. B. 1974 Nucl. Phys. A, 230, 1

Bodmer, A. R., & Usmani, Q. N. 1987, Nucl. Phys. A, 468, 653

Bodmer, A. R., & Usmani, Q. N. 1988, Nucl. Phys. A, 477, 621

Brown, G. E., Kubodera, K., Page, D., & Pizzochero, P. 1988, Phys. Rev. D, 37, 2042

Brown, G. E., Lee, C-H., Rho, M., & Thorsson, V. 1994 Nucl. Phys. A, 567, 937

Chrien, R. E., & Dover, C. B. 1989, Ann. Rev. Nuc. Part. Sci., 39, 227

Cook, G. B., Shapiro, S. L., & Teukolsky, S. A. 1992, ApJ, 398, 203

Cook, G. B., Shapiro, S. L., & Teukolsky, S. A. 1994, ApJ, 424, 823

Elgarøy, Ø., Engvik, L, Hjorth-Jensen, M, & Osnes, E. 1996, Nucl. Phys. A, 604, 466

Ellis, P. J., Lattimer, J. M., & Prakash, M. 1997 1997 Comments Nucl. Part. Phys. 22, 63

Feynman, R. P., Metropolis, N., & Teller, E. 1949, Phys. Rev., 75, 1561

Friedman, E., Gal, A, & Batty, C. J. 1994, Nucl. Phys. A, 579, 518

Friedman, J. F., Isper, J. R., & Parker, L. 1986, ApJ, 304, 115

Gibson, B. F., & Hungerford, E. V. 1995, Phys. Rep., 257, 349

Glendenning, N. K. 1985, ApJ, 293, 470

Glendenning, N. K. 1992, Phys. Rev. D, 46, 1274

Glendenning, N. K. 1996, Compact Stars, (New York: Springer)

Glendenning, N. K., & Moszkowski, S. A. 1991, Phys. Rev. Lett., 67, 2414

Glendenning, N. K., Pei, S., & Weber, F. 1997, Phys. Rev. Lett., 79, 1603

Haensel, P., & Zdunik, J. L. 1989, Nature, 340, 617

Haensel, P., & Gnedin, O. Yu. 1994, A&A, 290, 458

Huber, H., Weber, F., Weigel, M. K., & Schaab, Ch. 1998, Int. J. Mod. Phys. E7, 301

Kaplan, D. B., & Nelson, A. E. 1986, Phys. Lett. B, 175, 57

Keil, W., & Janka, H-T. 1995, A&A, 296, 145

Knorren, R., Prakash, M., & Ellis, P. J. 1995, Phys. Rev. C, 52, 3470

Lattimer, J. M., Prakash, M., Masak, D., & Yahil, A. 1990, ApJ, 355, 241

Lattimer, J. M., & Swesty, F. D. 1991, Nucl. Phys. A, 535, (1991) 331

Lattimer, J. M., Van Riper, K. A., Prakash, M., & Prakash, M. 1994, ApJ, 425, 802

Lorentz, C. P., Ravenhall, D. G., & Pethick, C. J. 1993, Phys. Rev. Lett., 70, 379

Mareš, J., Friedman, E., Gal, A., & Jennings, B. K. 1995, Nucl. Phys. A, 594, 311

Maxwell, O. V. 1987, ApJ, 316, 691

Millener, D. J., Dover, C. B., & Gal, A. 1988, Phys. Rev. C, 38, 2700

Miller, M. C., Lamb, F. K., & Cook, G. B. 1998, ApJ, 1998, 509 (in press)

Moszkowski, S. A. 1974, Phys. Rev. D, 9, 1613

Ögelman, H. 1995, in *The Lives of the Neutron Stars*, eds. M. A. Alpar, Ü. Kizilogu & van Paradijs, J. (Dordechet: Kluwer), 101.

Olesen, M. L., & Madsen, J. 1994, Phys. Rev. D, 49 2698

Page, D. 1995, Revi. Mex. Fis., 41, Supl. 1, 178

Pandharipande, V. R. 1971a, Nucl. Phys. A, 178, 123

Pandharipande, V. R. 1971b, Nucl. Phys. A, 174, 641

Pandharipande, V. R., Pines, D., & Smith, R. A. 1976, ApJ, 208, 550

Pandharipande, V. R., & Smith, R. A. 1975, Phys. Lett. B, 59, 15

Pandharipande, V. R., Pethick, C. J., & Thorsson, V. 1995, Phys. Rev. Lett., 75, 4567

Pines, D., & Alpar, M. A. 1985, Nature, 316, 27

Prakash, M., Prakash, M., Lattimer, J. M., & Pethick, C. J. 1992, ApJ, 390, L77

Prakash, M. 1994, Phys. Rep., 242, 297

Prakash, M. et al. 1997, Phys. Rep., 280, 1

Schaab, Ch., Weber, F., Weigel, M. K., & Glendenning, N. K. 1996, Nucl. Phys. A, 605, 531

Schaab, Ch., et al. 1997, A&A, 321, 591

Schaab, Ch., Balberg, S., & Schaffner-Bielich, J. 1998, ApJ, 504, L99

Schaffner, J., et al. 1994, Phys. Lett. B, 324, 268

Schaffner, J., & Mishustin, I. N. 1996, Phys. Rev. C, 53, 1416

Serot, B. D., & Walecka, J. D. 1980, Phys. Lett. B, 87, 172

Shapiro, S. L., & Teukolsky, S. A. 1983, Black Holes, White Dwarfs and Neutron Stars, (New York: Wiley)

van der Klis, M. 1998, *The Many Faces of Neutron Stars*, Proc. of Nato ASI, eds. R. Buccheri, J. van Paradijs, & M. A. Alpar, (Dordechet: Kluwer)337

Waas, T., Brockmann, R., & Weise, W. 1997, Phys. Lett. B., 405, 215

Weber, F., & Weigel, M. K. 1989, Nucl. Phys. A, 505, 779

Wiringa, R. B., Fiks, V., & Fabrocini, A. 1988, Phys. Rev. C, 38, 1010

This preprint was prepared with the AAS IATEX macros v4.0.

Fig. 1.— Relative fractions of the equilibrium composition of neutron star matter as a function of the baryon density, for EOS 2: (a) nuclear matter (b) matter with nucleons and all hyperons (c) matter with nucleons,  $\Lambda$  and  $\Xi$  hyperons but no  $\Sigma$ 's.

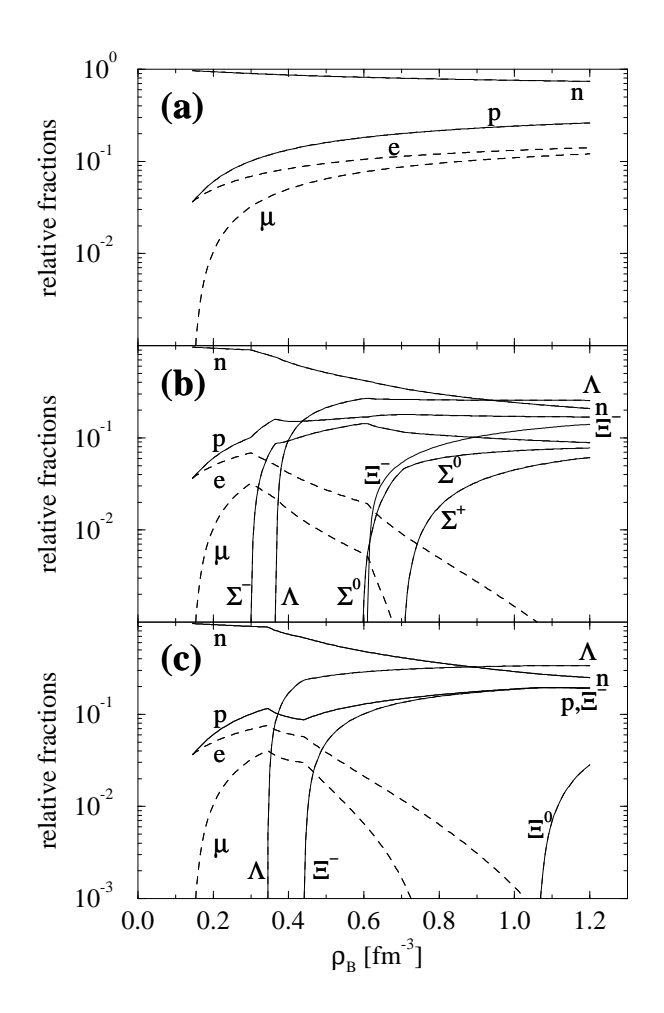


Fig. 2.— Equations of State for model 1 (thick lines) and model 2 (thin lines). The equations correspond to nuclear matter (solid lines), matter with nucleons and all hyperons (dashed lines), and matter with nucleons,  $\Lambda$  and  $\Xi$  hyperons but no  $\Sigma$ 's. (dot-dashed lines)

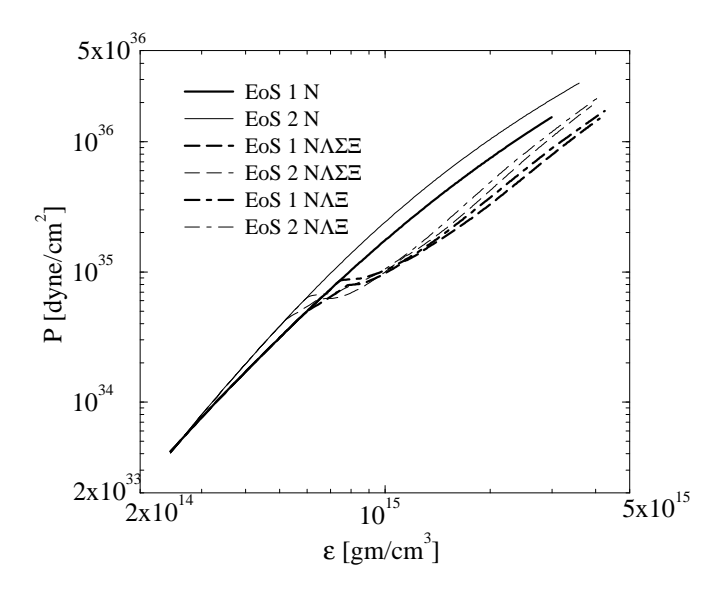


Fig. 3.— Static neutron star masses (in units of  $M_{\odot}$ ) as a function of the central energy density,  $\varepsilon_c$ , for the equations of state presented in Fig. 2. All lines as indicated in Fig. 2.

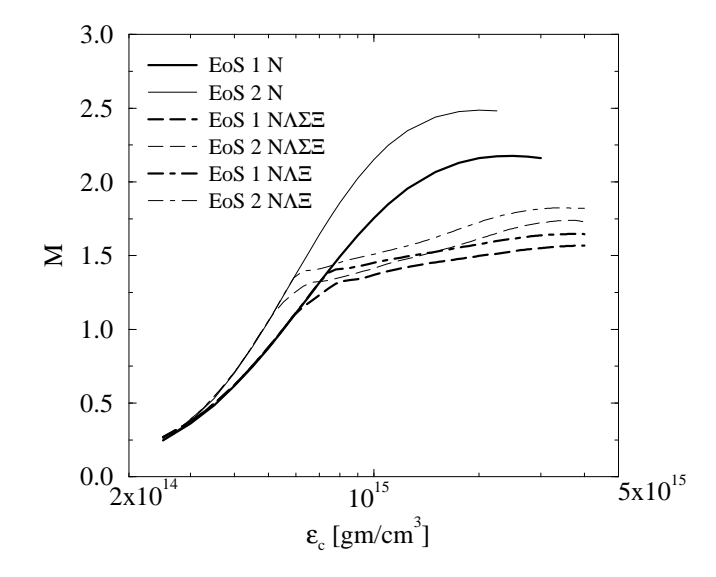


Fig. 4.— Radius vs. gravitational mass (in units of  $M_{\odot}$ ) relations for static neutron stars calculated with EOS 1 (thick solid line) and EOS 2 (thin solid line), and for the nuclear matter equations FPS, A, AU and L (see text for details).

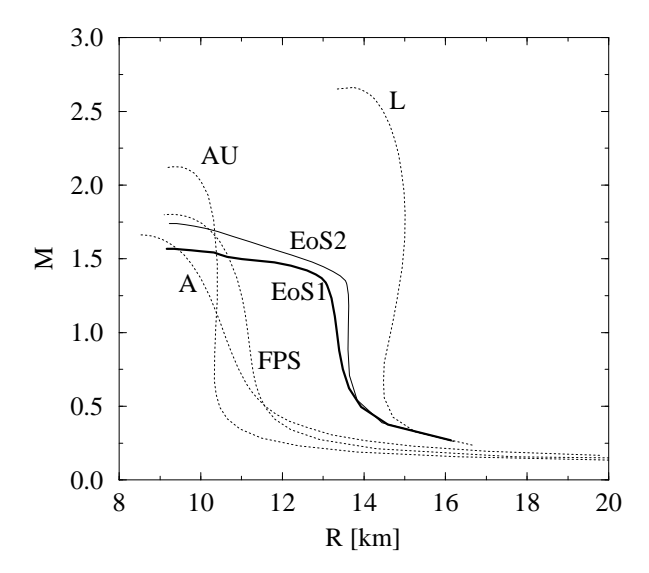


Fig. 5.— Constant rest mass sequences for EOS 2 showing the angular velocity,  $\Omega$ , as a function of the angular momentum, J. Selected sequences are labeled by the value of the rest mass, and the sequence which has a static gravitational mass of 1.4  $M_{\odot}$  is marked with an asterisk. The mass shed limit is the bold dashed line and the quasi-radial stability limit is denoted by the thin dashed line. The inset shows an expanded view of the region near the maximum mass model (open circle) and shows the location of the maximum  $\Omega$  model located at the intersection of the mass shed and stability limit.

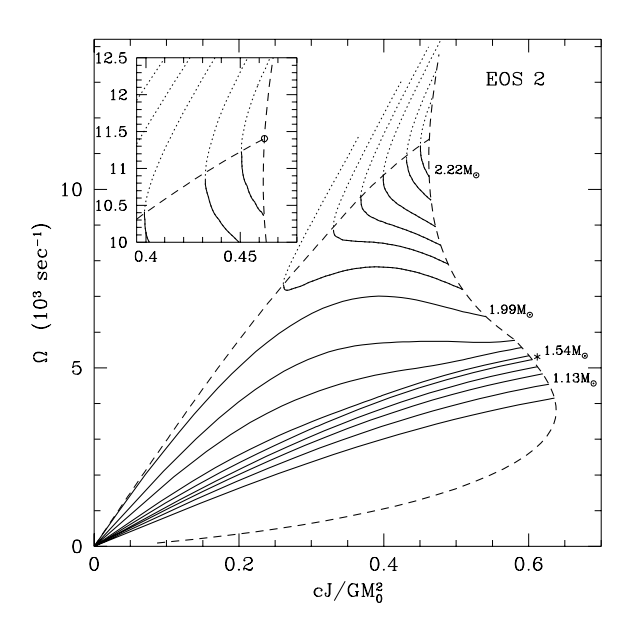


Fig. 6.— The adiabatic index,  $\gamma$ , for EOS 2 (solid line), the EOS with hyperons of Glendenning (1996) (dashed line) and the nuclear matter equation FPS (dot-dashed line), as a function of the mass-energy density.

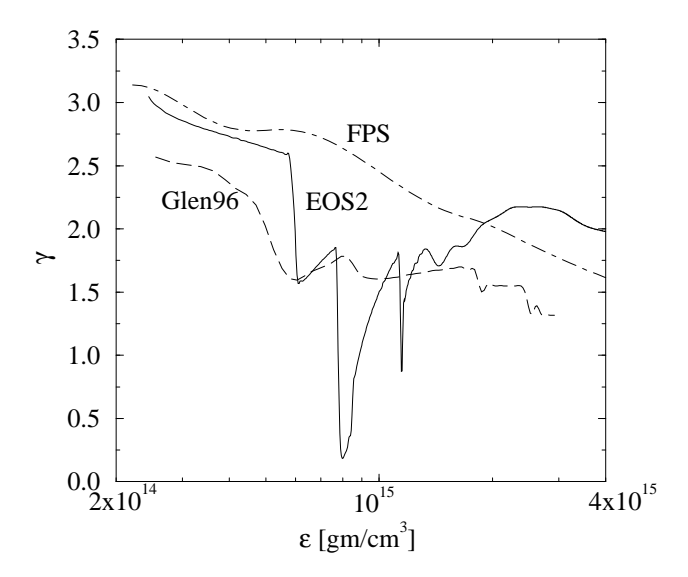


Fig. 7.— Constant rest mass sequences for EOS 2 showing the angular velocity,  $\Omega$ , vs. the gravitational Mass. The filled circles with error bars for the mass are the observed values of mass and angular velocity for several binary pulsars (see Cook et al. 1994). The vertical long-dashed line is the suggested lower limit of 1.55  $M_{\odot}$  on the mass of Vela X-1. The horizontal long-dashed line is the angular velocity of the millisecond pulsar PSR 1937+21.

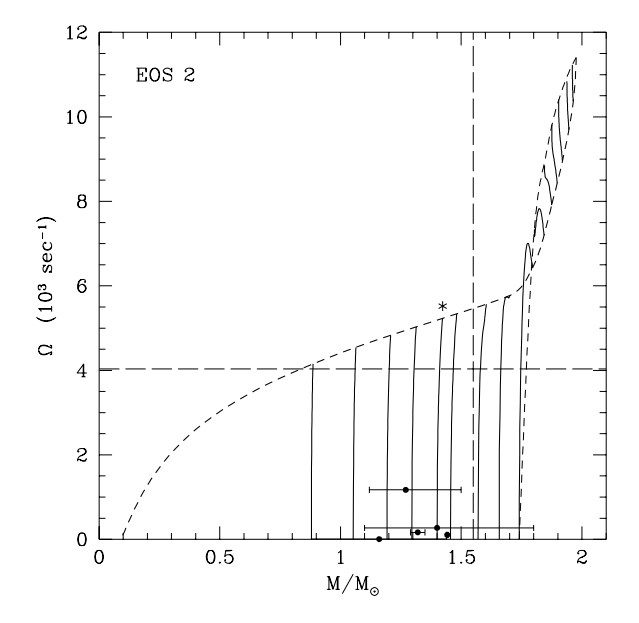


Fig. 8.— Fractional moment of inertia of the inner crust,  $I_{icr}/I_{tot}$ , as a function of the static mass (in units of  $M_{\odot}$ ) for EOS 1, EOS 2 (with and with out  $\Sigma$  hyperons, marked as in Fig. 2), and the nuclear matter equations FPS, A, AU and L. The thin dashed horizontal line corresponds to the observational constraint of the Vela 1978 glitch,  $I_{icr}/I_{tot} \ge 0.024$ .

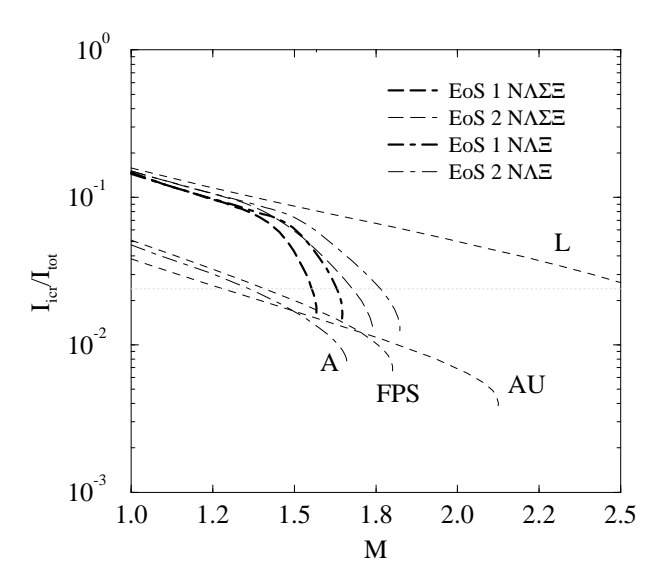


Fig. 9.— The electron chemical potential,  $\mu_e$ , for EOS 1 (thick lines) and EOS 2 (thin lines). The curves correspond to nuclear matter (solid line, identical for both equations), matter with nucleons and all hyperons (dashed lines) and matter with nucleons,  $\Lambda$  and  $\Xi$  hyperons but no  $\Sigma$ 's (dot-dashed lines).

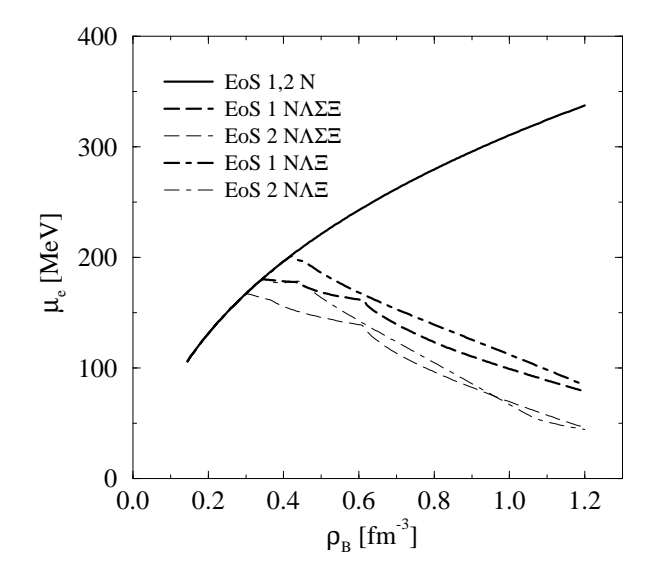


Fig. 10.— Energy per baryon, E/A, for baryonic matter (thick lines) and for quark matter of identical composition (thin lines) as a function of the baryonic density. The baryonic matter is calculated with EOS 1 (and the composition corresponds to the equilibrium composition of this equation). The quark matter is calculated with the MIT bag model with (a) B=100 MeV fm<sup>-3</sup>,  $\alpha_c=0$  (b) B=70 MeV fm<sup>-3</sup>,  $\alpha_c=0.3$ . The solid lines are nuclear matter and the corresponding two-flavor quark matter; the dashed lines are the baryonic matter with hyperons and the corresponding three-flavor quark matter.

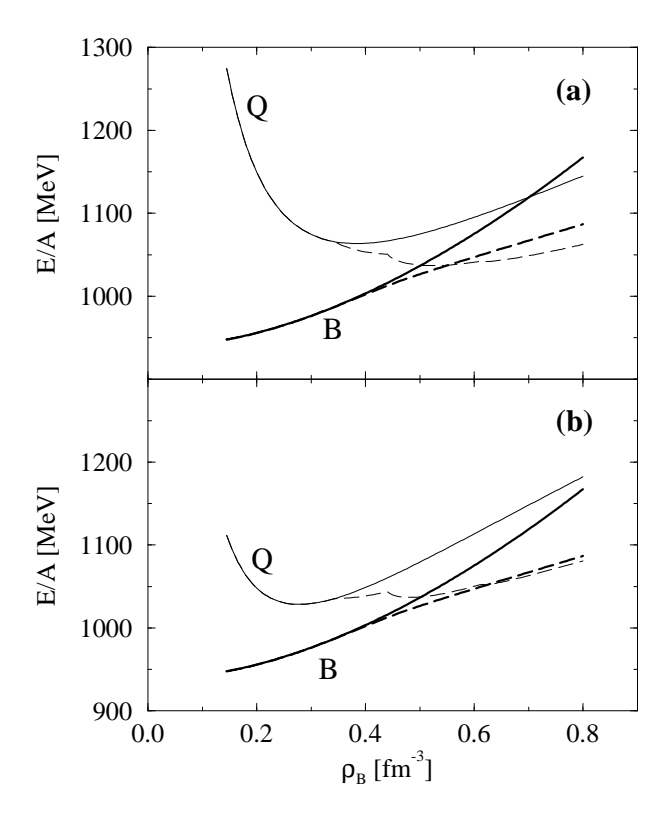


Table 1. Quantum numbers of the baryons in the spin  $\frac{1}{2}$  octet: mass (in MeV/ $c^2$ ), strangeness, and isospin projection

	mass	S	$I_3$
$\begin{array}{c} \mathbf{p} \\ \mathbf{n} \\ \mathbf{\Lambda} \\ \Sigma^{+} \end{array}$	938.3 939.6 1115.6 1189.4	0 0 -1 -1	$-\frac{\frac{1}{2}}{\frac{1}{2}}$ 0
$\Sigma^{0}$ $\Sigma^{-}$ $\Xi^{0}$ $\Xi^{-}$	1192.5 1197.3 1314.9 1321.3	-1 -1 -1 -2 -2	$0$ $-1$ $\frac{1}{2}$ $-\frac{1}{2}$

Table 2. Coefficients for the potential energy density term in Eq. (A2)

	EOS 1	EOS 2		EOS 1	EOS 2
K [MeV]	240	320	$a_{\Sigma N}^{\dagger}$	-481.3	-354.8
$\gamma$	4/3	5/3	$b_{\Sigma N}{}^{\dagger}$	214.2	214.2
$\theta$	5/3	2	$c_{\Sigma N}^{\ddagger}$	499.6	484.3
$w^{\star}$	223.6	220	$a_{\Xi N}^{\dagger}$	-410.2	-303.1
$a_{NN}^{\dagger}$	-690.0	-481.7	$b_{\Xi N}{}^{\dagger}$	0	0
$b_{NN}{}^{\dagger}$	107.1	107.1	$c_{\Xi N}^{\ddagger}$	415.3	394.6
${c_{NN}}^{\ddagger}$	744.6	715.5	$a_{YY}^{\dagger}$	-676.1	-513.3
$a_{\Lambda N}{}^{\dagger}$	-481.3	-354.8	$b_{\Sigma\Sigma}{}^{\dagger}$	214.2	214.2
$b_{\Lambda N}{}^{\dagger}$	0	0	$b_{\Xi\Xi}{}^{\dagger}$	0	0
$c_{\Lambda N}^{\ddagger}$	499.6	484.3	$c_{YY}^{\ddagger}$	658.1	764.7

 $<sup>^\</sup>dagger \rm MeV~fm^3$ 

 $<sup>^{\</sup>ddagger} \rm MeV~fm^{3\gamma}$ 

<sup>\*</sup>MeV fm $^{3\theta}$